Journal of The Electrochemical Society

The Electrochemical Society
Advancing solid state & electrochemical science & technology

Review—Recent Progress in Flexible and Stretchable Piezoresistive Sensors and Their Applications

To cite this article: Jing Li *et al* 2020 *J. Electrochem. Soc.* **167** 037561

Journal of The Electrochemical Society, 2020 **167** 037561

Review—Recent Progress in Flexible and Stretchable Piezoresistive Sensors and Their Applications

Jing Li,[1,=,z] Lichen Fang,[2,3,=] Bohan Sun,[2,3] Xixing Li,[1] and Sung Hoon Kang[2,3,z]

[1]*School of Mechanical Engineering, Hubei University of Technology, Wuhan, Hubei 430068, People's Republic of China*
[2]*Department of Mechanical Engineering, Johns Hopkins University, Baltimore, Maryland 21218, United States of America*
[3]*Hopkins Extreme Materials Institute, Johns Hopkins University, Baltimore, Maryland 21218, United States of America*

The recent advances in wearable electronics and intelligent human-machine interface systems have garnered great interests in electromechanical sensors, which can measure and quantify physical stimuli. Among different types of electromechanical sensors, piezoresistive sensors have been extensively investigated due to the excellent sensitivity, simple construction, and durability. Especially, there have been remarkable developments of flexible and stretchable piezoresistive sensors for wearable devices by investigating novel material/structural strategies to obtain highly sensitive piezoresistive sensors with skin-like flexibility. Here, we give a comprehensive overview of the recent progress in flexible and stretchable piezoresistive sensors and their applications. Based on the material composition and structural characteristics, the piezoresistive sensors are categorized into three types—conductive polymeric composite, porous conductive material, and architected conductive material. Subsequently, we have summarized their transduction mechanisms, fabrication processes, sensing performances, and applications. Finally, we have discussed current challenges and future opportunities for piezoresistive sensors.
 [DOI: 10.1149/1945-7111/ab6828]

Manuscript submitted September 19, 2019; revised manuscript received December 9, 2019. Published February 3, 2020. *This paper is part of the JES Focus Issue on Sensor Reviews.*

With the growing interest of environmental and physiological information perception, there have been active research on flexible and stretchable electromechanical pressure/strain sensors due to their capabilities of transduction of physical stimuli to measurable electrical signals.[1–12] Recently, the rapid development of the electrical sensing techniques and fabrication technologies have contributed to the significant progress in the investigation of advanced functional materials/structures for the electromechanical sensing applications.

To achieve the conversion between mechanical and electrical signals, researchers have utilized the generation of charges[13–16] and the variation of capacitance[17–19] or resistance[20–22] upon mechanical loading (e.g. pressure, strain). Therefore, the transduction mechanisms of the electromechanical sensors can be generally classified into piezoelectricity/triboelectricity, piezocapacitance, and piezoresistivity. The piezoelectric pressure sensors are based on the piezoelectric effect caused by the change of the internal polarization of the inorganic piezoelectric materials (e.g., lead zirconate titanate (PZT),[23] barium titanate (BTO)[24] and zinc oxide(ZnO)[25]), organic piezoelectric polymers (e.g., polyvinylidene fluoride (PVDF)[26] and poly(l-lactic acid) (PLLA)[27]), or piezoelectric composites.[28] And, for the triboelectric pressure sensors, they produce electric charges due to the triboelectric effect, which is a type of contact electrification.[15] Benefiting from the unique charge generation feature, piezoelectric and triboelectric pressure sensors can provide sustainable power for themselves as self-powered sensors.[29] But, they are limited in sensing subtle and/or static mechanical loadings. Capacitive sensors are constructed by a deformable dielectric material with parallel plates on the top and bottom surfaces. Under pressure loading, the deformation of the sandwiched dielectric material leads to the distance change of the parallel plates, resulting in the capacitance change.[18] Capacitive sensors possess high sensitivity and low hysteresis, and can detect both static and dynamic loadings. However, the capacitance change is usually on the order of picofarads (pF) range. The relatively small capacitive variation impedes the further improvement of the corresponding pressure sensor, and requires careful circuit design to minimize the effects of parasitic capacitance.[30] The piezoresistive sensors are based on the piezoresistive effect, which is the change in the electrical resistivity of materials when pressure is applied. Owing to the simple construction and readout circuits, the piezoresistive sensors are low cost, durable, and robust with high-resolution to both static and dynamic pressure/strain.[3,5]

Importantly, among these transduction approaches, flexible and stretchable electromechanical sensors with high sensitivity and fast response time are essential characteristics for successful monitoring of real-time physical stimuli. In Fig. 1, we have summarized the pressure sensitivity and response time of some of the recently reported piezoresistive,[31–36] piezoelectric[37–40] and capacitive sensors.[41–45] Compared to the plotted piezoelectric and capacitive sensors, piezoresistive sensors showed outstanding pressure sensitivities with a relatively fast response time. Piezoresistive sensors can offer linear electromechanical sensing performance over wide strain ranges, which enables the reliable sensing performance for practical applications.[46,47] Owing to their simplicity in device structures, high sensitivity, and linearity, piezoresistive sensors are most widely used in commercial micro-electromechanical systems (MEMS) devices.[48] Not surprisingly, flexible and stretchable piezoresistive sensors are the promising candidates and indispensable parts for future generations of wearable intelligent electronics.[2,49,50] Recently, there have been many exciting progress in the development of flexible and stretchable piezoresistive materials for wearable sensing applications.

In this review paper, we aim to present a comprehensive overview of the flexible and stretchable piezoresistive sensors. First, we categorize the recently reported piezoresistive sensors into three types and summarize their characteristic features and working mechanisms. Second, we describe the detailed fabrication processes, electromechanical sensing performances and applications of each type of piezoresistive sensors. Finally, we conclude this review paper with the grand challenges and future perspectives of the piezoresistive sensors for further study.

Types of Advanced Materials/Structures for Piezoresistive Sensors

Traditionally, piezoresistive sensors are based on rigid and brittle inorganic materials (such as polycrystalline metals and single crystal silicon and nitride materials), which have very limited mechanical flexibility.[51,52] However, for wearable electronic applications, the piezoresistive sensors are required to possess high stretchability and

[=]These authors contributed equally to this work.
[z]E-mail: lijing@hbut.edu.cn; shkang@jhu.edu

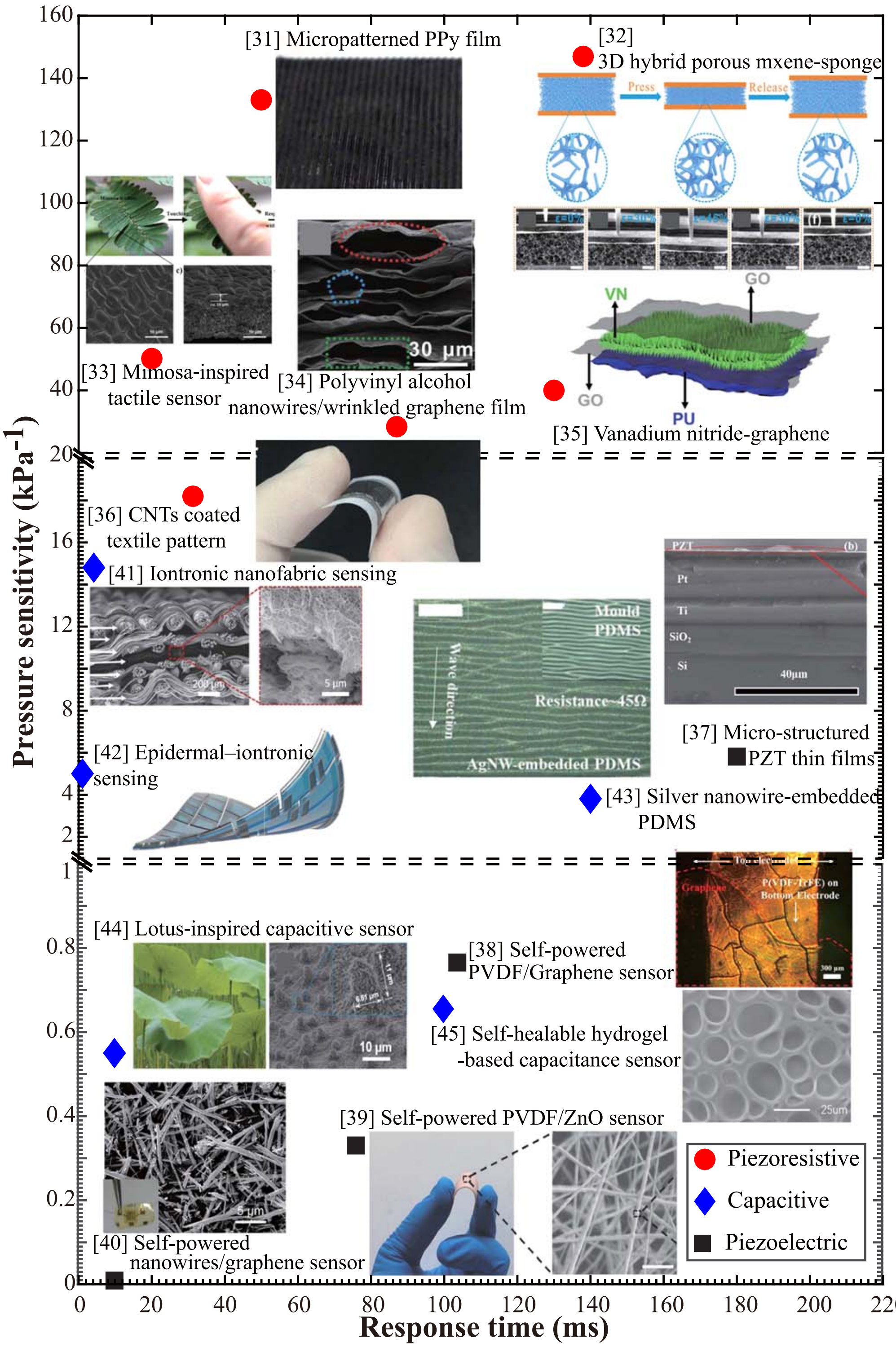

Figure 1. Comparison of pressure sensitivity and response time among the recently developed piezoresistive,[31–36] piezoelectric[37–40] and capacitive[41–45] sensors. Copyright 2014, Nature Publishing Group;[31] Copyright 2018, Elsevier;[32] Copyright 2015, John Wiley and Sons;[33] Copyright 2017, John Wiley and Sons;[34,41,42] Copyright 2019, Springer;[35] Copyright 2017, John Wiley and Sons;[36] Copyright 2019, Royal Society of Chemistry;[37] Copyright 2019, American Chemical Society;[38] Copyright 2019, Elsevier;[39] Copyright 2017, American Chemical Society;[40] Copyright 2015, Royal Society of Chemistry;[43,45] Copyright 2016, John Wiley and Sons.[44]

conformability, as well as the capability to detect subtle loadings over a wide strain range.[1,2,5,6,8] To achieve both high piezoresistive sensitivity and mechanical flexibility, Jeong group[53] and Youngblood group[54] reported that flexible piezoresistive sensors could be fabricated by utilizing the conductive nanomaterials as the functional sensing elements coupled with stretchable polymeric matrices. Besides, as Kim group[10] and Rogers group[55] reported, porous conducive materials and conductive materials with geometries designed to enhance sensing performance are other promising approaches to realize a unique combination of high mechanical compliance and sensitivity. Based on the aforementioned stretchable material design strategies, great achievements have been reported in the investigation of advanced materials/structures for flexible and stretchable piezoresistive sensors. In this paper, we categorize these materials/structures into three types based on their structural and compositional characteristics, as shown in Fig. 2: (1) *conductive polymeric composite*—viscoelastic polymer matrix dispersed with conductive material; (2) *porous conductive material*—conductive material with three-dimensional interconnected porous structure; (3) *architected conductive material*—conductive material system with carefully designed geometry. Table I lists several recently reported flexible and stretchable piezoresistive sensors in terms of sensitivity, response time, pressure detection limit, and their applications based on these three categories.

The principle transduction mechanism for the aforementioned material/structure is the contact area variation of electrical conductors during transient deformations.[2,72,73] However, each of these transduction methods has its own features: (1) The sensing mechanism of the conductive polymeric composites is attributed to the mobility of conductive fillers within the viscoelastic polymer matrix; under compressive force, the temporarily contacted conductive fillers would form more conductive pathways, leading to the change of resistance (Fig. 3a);[74] (2) For the porous conductive materials, the sensing mechanism is due to contact and separation of the conductive elements within the porous matrix; under compressive deformation, the pores are condensed and the conductive materials contact each other, resulting in the increase in conductive contact areas and the resistance change (Fig. 3b);[75] (3) Additionally, the architected conductive materials have carefully designed and fabricated microstructures, which have large contact area changes upon small external loadings, leading to a high sensitivity (Fig. 3c).[76,77]

In the following sections, the detailed fabrication processes, performances, and applications of the categorized three types of piezoresistive sensors are discussed.

Conductive Polymeric Composite-Based Piezoresistive Sensors

The polymeric composites filled with conductors can combine appropriate electrical properties of the conductive fillers with excellent mechanical compliance of the flexible matrices. Here, we summarized the recent progress of conductive polymeric composite-based piezoresistive sensors in terms of the widely used conductive fillers, including CNTs, graphene, and other conductive materials (e.g., metallic materials, conductive polymers).

CNT-based conductive polymeric composites.—CNTs are layered cylindrical molecules of carbon atoms, which exhibit high electrical conductivity and exceptional mechanical properties.[78,79] These properties make them widely used as a conductive filler for conductive polymeric composite-based piezoresistive sensors. Many commercially available polymers and elastomers including poly (dimethylsiloxane) (PDMS),[66,80,81] Ecoflex,[82,83] polyurethane (PU),[84,85] epoxy,[86,87] Poly(vinylidene fluoride) (PVDF),[88] and polymethyl methacrylate (PMMA)[56] are used as polymeric matrices.

PDMS is a silicone rubber with low Young's modulus, intrinsic extensibility, high transparency, and excellent stability, and can be easily prepared in a laboratory. These advantages make the PDMS as

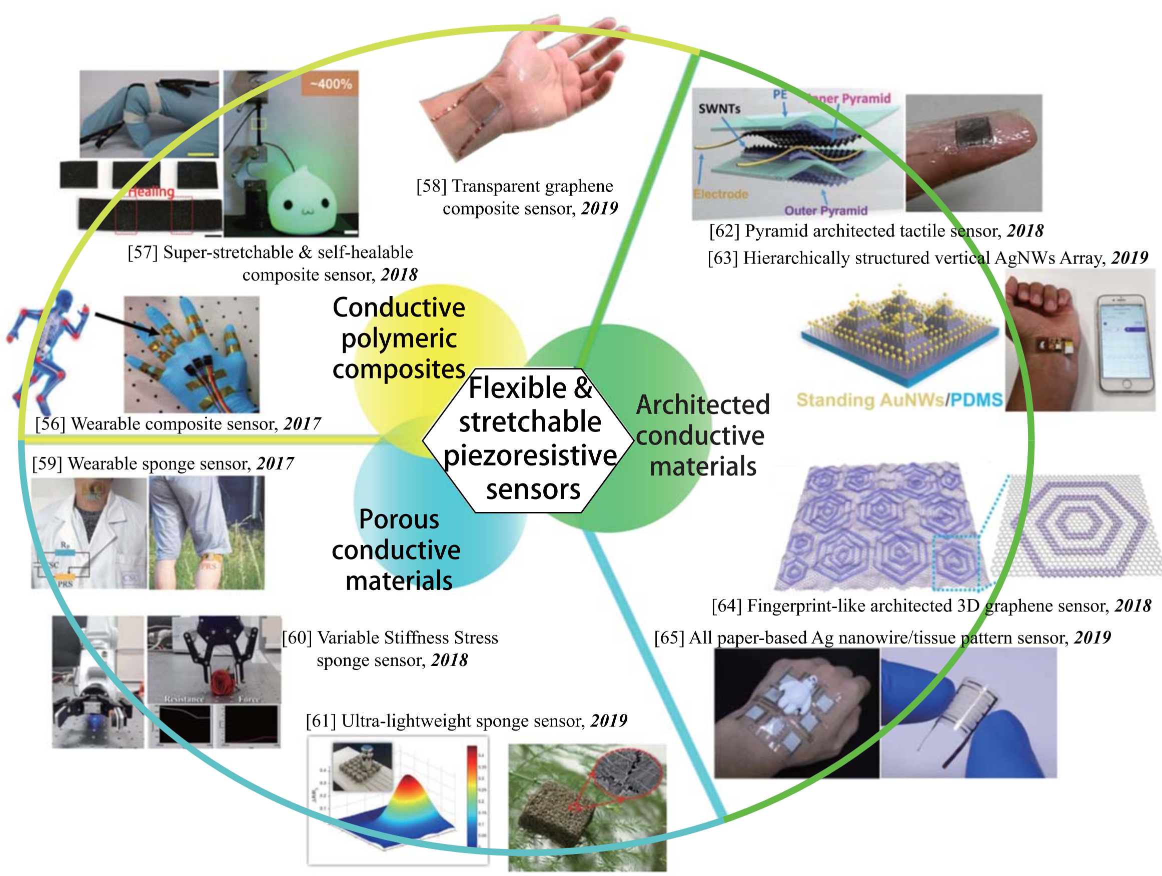

Figure 2. The categorization of recently reported advanced material/structure strategies for flexible and stretchable piezoresistive sensors based on their structure and composition characteristics. Reproduced with permission from Ref. 56, Copyright 2017, John Wiley and Sons. Reproduced with permission from Ref. 57, Copyright 2018, John Wiley and Sons. Reproduced with permission from Ref. 58, Copyright 2019, American Chemical Society. Reproduced with permission from Ref. 59, Copyright 2017, John Wiley and Sons. Reproduced with permission from Ref. 60, Copyright 2018, John Wiley and Sons. Reproduced with permission from Ref. 61, Copyright 2019, American Chemical Society. Reproduced with permission from Ref. 62, Copyright 2018, John Wiley and Sons. Reproduced with permission from Ref. 63, Copyright 2019, American Chemical Society. Reproduced with permission from Ref. 64, Copyright 2018, Springer. Reproduced with permission from Ref. 65, Copyright 2019, American Chemical Society.

Table I. **Summary of recently reported flexible and stretchable piezoresistive sensors and their sensing performances.**

Piezoresistive sensor categories	Materials	Sensitivity	Response time	Detection limit	Application	References
Conductive polymeric composite	Graphene/PDMS	44.5 kPa^{-1}	—	—	Human pulse detection	58
Conductive polymeric composite	SWNTs/PDMS	1.8 kPa^{-1}	$<$10 ms	0.6 Pa	Small muscle movement	66
Conductive polymeric composite	Metal particle/PU	2.46 kPa^{-1}	30 ms	—	Finger motion	67
Porous conductive material	MXene/PVA NWs	147 kPa^{-1}	138 ms	9 Pa	Human physiology detection	32
Porous conductive material	Vanadium nitride-graphene	40 kPa^{-1}	130 ms	—	Health monitoring	35
Porous conductive material	Carbonized melamine	100.3 kPa^{-1}	—	3 Pa	Wrist pulse detection	68
Porous conductive material	Graphene	10 kPa^{-1}	0.2 ms	0.1 Pa	Subtle loading	69
Architected conductive material	Polypyrrole	133 kPa^{-1}	50 ms	1 Pa	Subtle loading	31
Architected conductive material	Au deposited PDMS	50.7 kPa^{-1}	20 ms	—	Tactile sensing	33
Architected conductive material	Au micropillar array	17 kPa^{-1}	—	2 Pa	Subtle loading	70
Architected conductive material	Structured PDMS/Ag NWs	2.3 kPa^{-1}	100 ms	—	Small muscle movement	71

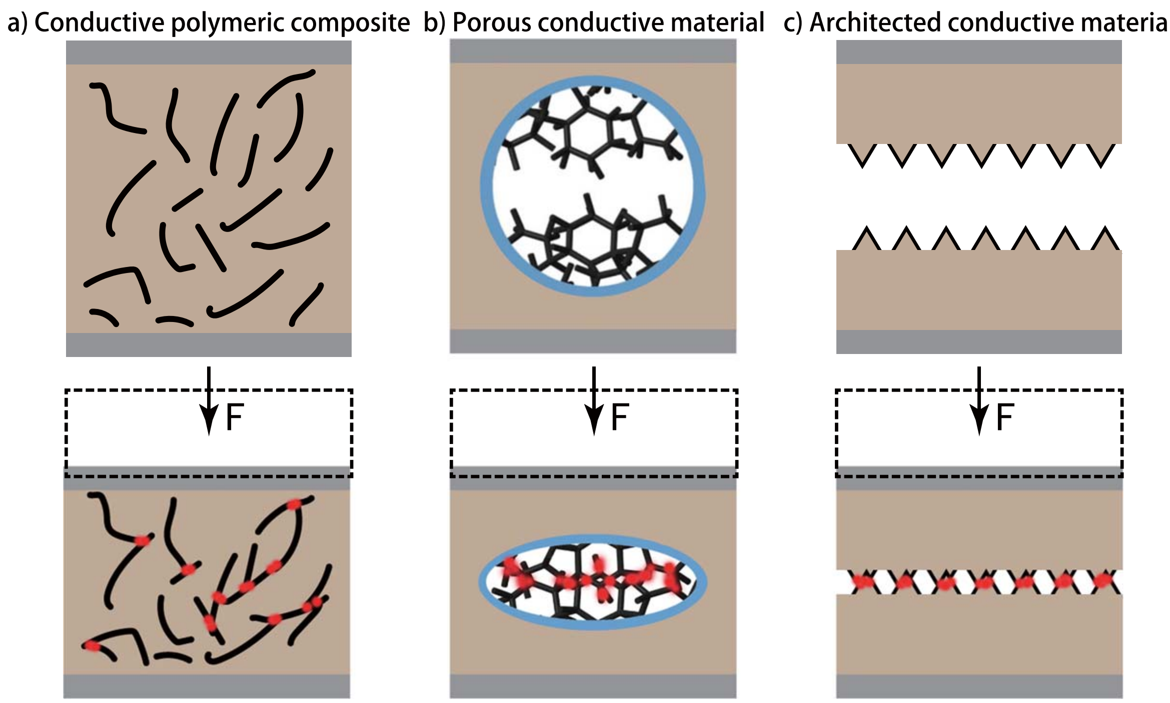

Figure 3. The schematic images of material/structure strategies and transduction methods for piezoresistive sensors: (a) conductive polymeric composite, (b) porous conductive material, (c) architected conductive material.

the first option of the polymer matrix for the composite toward flexible electronics.[17,89] Conventionally, the CNTs are randomly dispersed in the PDMS monomer followed by adding the curing agent.[90] However, the sensitivity of the CNT/PDMS composite is low and cannot detect the tactile pressure range (<1 kPa). Recently, lots of studies have been conducted to increase the sensing performance of CNT/PDMS composite. For example, Wang et al.[91] constructed self-segregated structures to form dense conductive CNT networks in PDMS matrix, resulting in the enhanced electrical conductivity and piezoresistive sensing performance (Fig. 4a); the self-segregated composite not only showed 7.4 times higher gauge factor (GF = $(\Delta R/R)/\varepsilon$, where $\Delta R/R$ is the fractional resistance change and ε is the applied mechanical strain) compared with that of conventional samples, but also had higher compression modulus and strength. Zheng et al.[92] used a solution mixing-casting method to mix PDMS with hybrid CNT and carbon black (CB) conductive fillers; their works demonstrated that the bridged and overlapped hybrid CNT-CB nanofiller structure successfully improved the sensitivity and electrical conductivity of the composite; based on the as-demonstrated composite, the authors also assembled wearable sensors to detect human joint motions.

Ultra-soft Ecoflex exhibits stretchability as high as that of human skin, and it is an environmentally stable polymer, which makes it suitable for electronic skin applications.[82] The CNT/Ecoflex composite-based sensors possess prominent stretchability. For example, Mai et al.[93] blended CNTs with Ecoflex matrix to fabricate ultra-stretchable and mechanically resilient self-standing piezoresistive sensors, which exhibited an elastic modulus as soft as human skin (Fig. 4b); the as-prepared sensor presented a linear electromechanical response up to 200% strain and high durability, which can also be easily adhered to human skin as a soft sensor for wearable real-time monitoring applications. Jiang et al.[83] integrated CNTs and Ecoflex into a stretchable sensor with interactive transmittance-changing and strain-sensing capabilities; due to the ultra-flexible mechanical properties of the Ecoflex, the composite film can be stretched up to 400% strain without breaking, which is suitable for monitoring daily activities with large displacement.

Moreover, CNT/PU, CNT/epoxy, CNT/PVDF, and CNT/PMMA composites are also widely used for flexible and stretchable piezoresistive sensors. PU, one of the most versatile materials, can be molded into complex shapes and incorporated into various items.[95] Roh et al.[84] reported an environmentally benign water-based solution processing to fabricate stretchable, ultrasensitive CNT/PU composite sensors using single-wall CNTs and conductive elastomeric PU-PEDOT:PSS. The sensors have an optical transmittance of 62% in the visible range providing excellent optical transparency (Fig. 4c), which can be invisibly mounted to human skin for small strain detection such as human facial laughing and crying expression. Additionally, epoxy resin has high bond strength, outstanding mechanical strength, and excellent chemical resistance, which make it suitable for applications.[96] Liu et al.[94] synthesized the CNT/epoxy composite by symmetric plasma-modified CNTs and epoxy resin (Fig. 4d). Due to the enhanced interfacial bonding of the functionalized CNTs, the CNT/epoxy composite showed remarkable mechanical peeling strength ($331.2\ \mathrm{N\ m^{-1}}$) and tensile toughness ($134.9\ \mathrm{J\ m^{-3}}$), as well as strain sensitivity with gauge factor of ∼4 up to 45% tensile strain. Moreover, PVDF composite sensors are promising for structural health monitoring applications from civil infrastructures to airplanes, due to their good resistance against radiation and chemical erosion.[97] Ke et al.[88] introduced a simple melt mixing method to construct strain-susceptible hybrid conductive networks in the CNT/PVDF composite, leading to enhanced electrical conductivity and piezoresistive sensitivity. Furthermore, PMMA has also been actively used in flexible electronics. Khanafer et al.[89] proposed a novel piezoresistive composite with aligned CNT-arrays inside the PMMA polymer matrix for stretchable piezoresistive sensors. The as-prepared transparent composite has high durability, stretchability, and electromechanical sensitivity.

Graphene-based polymeric composites.—Graphene is a two-dimensional (2D) material consisting of a monolayer of carbon atoms arranged in a hexagonal lattice. Owing to its extraordinary mechanical, electrical, and thermal properties, graphene has been intensively investigated and considered as a promising candidate for advancing flexible electronic devices.[98–101] As a well-studied

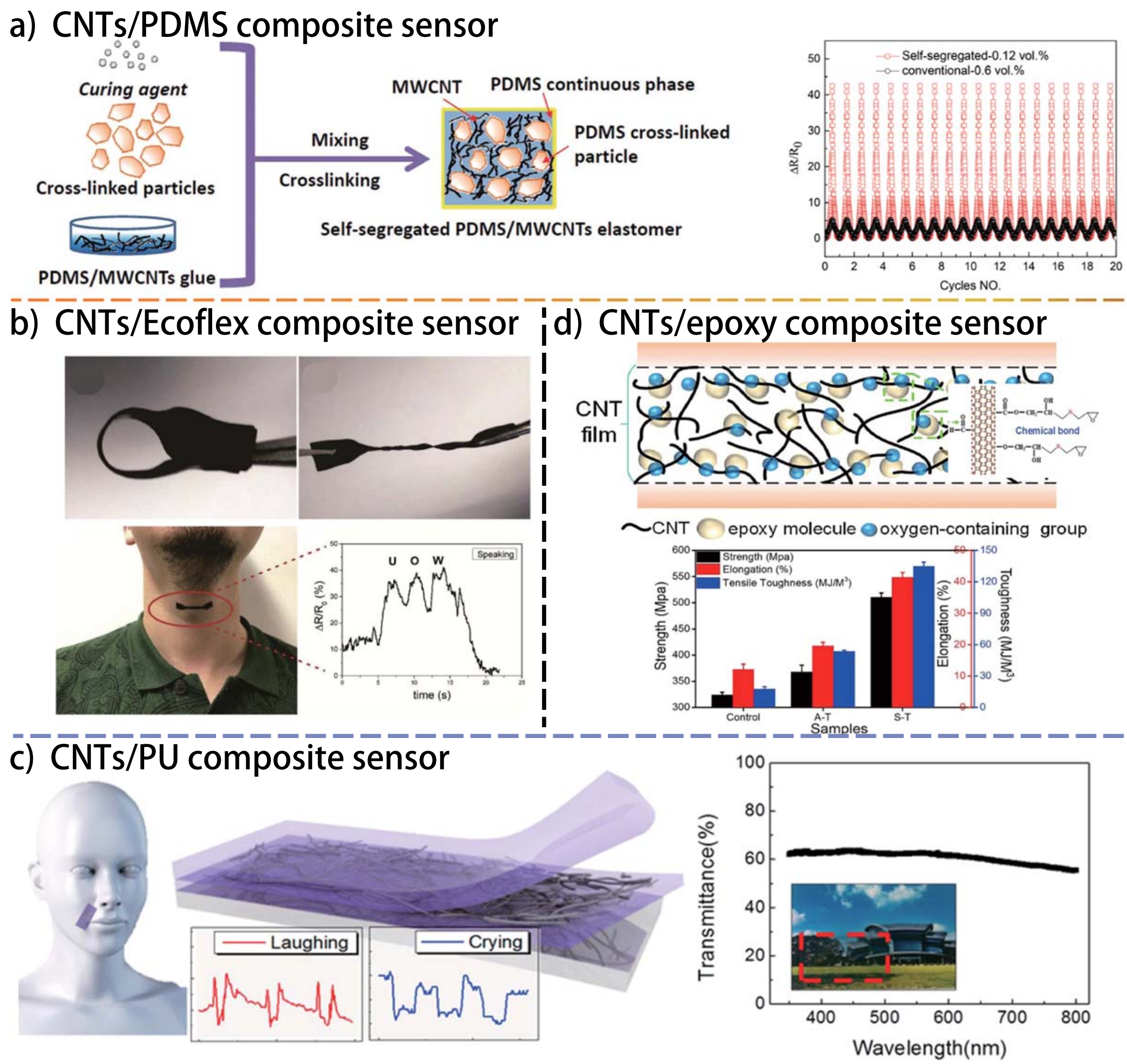

Figure 4. CNT-based polymeric composites for advanced flexible and stretchable piezoresistive sensors. (a) The schematic of the fabrication method for preparing self-segregated CNT/PDMS composite and the cyclic piezoresistive response of the self-segregated composite (red symbol and line) compared to conventional samples (black symbol and line).[91] Copyright 2017, Royal Society of Chemistry. (b) Photographs of the fully bent and twisted CNT-Ecoflex composite samples showing the ultra-high flexibility of the composite; Free-standing MWCNT-Ecoflex composite sensor placed on human neck for detection of speaking letters.[93] Copyright 2019, Elsevier. (c) Schematic illustration of stretchable CNTs/PU composite strain sensor attached to human skin for pressure sensing (laughing and crying); Transmittance spectra of this strain sensor to demonstrate the transparent feature.[84] Copyright 2015, American Chemical Society. (d) The plasma functionalized CNTs created a strong chemical bond with epoxy and this CNT/epoxy polymeric composite piezoresistive sensor presented ultra-high mechanical peeling strength and toughness.[94] Copyright 2019, Elsevier.

flexible electromechanical sensor, graphene-based polymeric composites incorporate graphene into elastomeric matrices such as PDMS,[102–104] Silly Putty,[105] PVDF,[106–108] Ecoflex,[109,110] PLA,[111] polysiloxane,[112] and other viscoelastic elastomers. Generally, graphene/polymer composite sensors possess higher sensitivity due to the high carrier mobility and large surface area of the 2D graphene fillers.[113] To further enhance the sensitivity of the graphene/polymer composite sensors, Yang et al.[114] added Ag nanoparticles to graphene-PDMS mixture by drop-casting, which are used to fill the gaps between randomly dispersed graphene sheets as "bridges" (Fig. 5a). The Ag nanoparticle-bridged graphene/PDMS composite simultaneously achieved high sensitivity with a strain gauge factor up to 475 and a broad sensing strain range of ∼14.5%. Owing to these outstanding piezoresistive performance, this piezoresistive composite sensor can be used to detect both subtle and intensive human activities including small-scale and large-scale motions. Besides, to address the overlapping issue of the 2D graphene sheet in composite materials, Wu et al.[115] and Luo et al.[116] utilized the structured 3D graphene foam fillers with tunable electrical conductivity and elasticity as an effective reinforcing agent to enhance the piezoresistive sensitivity and linear sensing range of the graphene/PDMS composite sensors, compared to conventional graphene/PDMS composites (Fig. 5b). Moreover, Huang et al.[117] developed a homogeneous graphene-PDMS mixture with appropriate rheological property of the slurry for 3D printing (Fig. 5c). The as-printed 3D graphene/PDMS composite displayed good mechanical properties, high sensitivity (gauge factor up to 448 at 30% strain), and fast electromechanical response time. This work has shown the enormous potential of graphene/PDMS composite for practical application in advancing flexible electronics.

Inspired by the fact that the sensing mechanism of the graphene/polymer composite is breaking and reforming the conductive network of mobile graphene fillers, Boland et al.[105] proposed that a lightly cross-linked polymer matrix with high viscous properties would enhance the mobility of the graphene fillers, resulting in super-high sensitivity. Based on this hypothesis, they embedded graphene in highly viscoelastic Silly Putty matrix (Fig. 6a). Due to the high mobility of the graphene nanosheets in the high viscosity

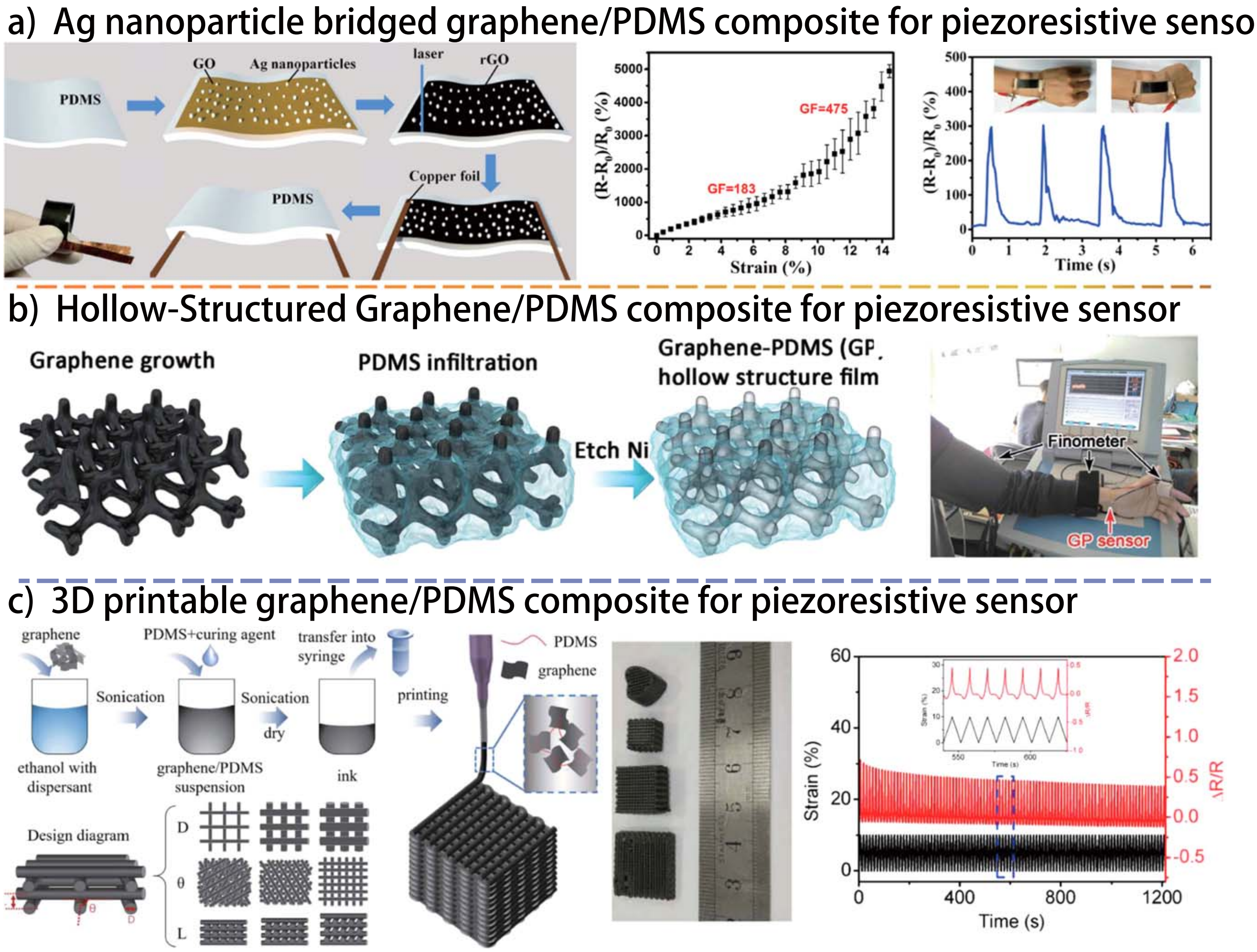

Figure 5. Graphene/PDMS composites for advanced flexible and stretchable piezoresistive sensors. (a) Illustrations of the fabrication and performances of Ag nanoparticle-bridged graphene/PDMS composite sensors that have a strain gauge factor up to 475 and can detect subtle and intensive human activities.[114] Copyright 2018, American Chemical Society. (b) The fabrication method of the hollow structured graphene/PDMS composite for piezoresistive sensor and the application in human pulse monitoring.[116] Copyright 2017, John Wiley and Sons. (c) Schematic of preparing a graphene-PDMS mixture for 3D printing and the real image of the as-printed graphene/PDMS composite with different parameters for piezoresistive sensing applications.[117] Copyright 2019, Elsevier.

Putty polymer matrix (Fig. 6b), this graphene/Putty composite displayed outstanding electromechanical features, such as dramatic change in resistivity with mechanical strain and temporal relaxation of electric resistance. The measured piezoresistive sensing gauge factor of this graphene/Putty composite is more than 500 (Fig. 6c) with ability to detect subtle pressures including static weight-loading and dynamic footsteps of a small spider (Fig. 6d). For the wearable electronic sensor applications, this composite is capable of monitoring finger joint motion and human breath (Fig. 6e).

Besides the example above, graphene/PVDF and graphene/Ecoflex composites are other promising candidates for flexible piezoresistive sensors. Costa et al.[106] fabricated PVDF polymeric composite with carbonaceous graphene oxide (GO) and reduced graphene oxide (rGO) by solution casting method. Although the sensitivity of as-prepared graphene/PVDF composite (strain gauge factor ∼11) is not particularly good compared to other works, the composite exhibited excellent linear correlation between the applied mechanical loading and the electrical resistance change, which is an essential feature for the measurement accuracy of the flexible electromechanical sensors. Moreover, to take full advantage of ultra-stretchability of the Ecoflex elastomer, Wang et al.[110] adopted vacuum-assisted filtration method to integrate graphene and Ecoflex with meandered zinc wires. The as-fabricated composite sensor possessed piezoresistive sensitivity with a detection range up to 150% tensile strain without any damage. Due to the flexibility of this graphene/Ecoflex composite sensor, it could be easily attached to a human joint for large motion sensing.

Furthermore, for some biomedical electronic applications, pressure sensors are directly implanted into biological organs. In this regard, these sensors are required to be biocompatible and biodegradable to avoid invasive removal surgery. So, Scaffaro et al.[111] fabricated graphene-based amphiphilic composite sensor using biodegradable polymer matrix, poly (lactic acid) (PLA)-Poly (ethylene-glycol) (PEG). To mimic the therapeutic property of natural skin, Zhao et al.[112] reported a self-healable graphene/polysiloxane composite sensor (sensitivity of 0.765 kPa^{-1}) based on the solid-liquid-solid transformation of the dynamic Diels-Alder bonds.

Other conductive material-based composites.—In addition to the conductive CNTs and graphene fillers, metallic materials (e.g., metal particles[67,118,119] and metal nanowires[45,120–123]) and other elastic conductive components[124–126] are also incorporated into flexible elastomers for advancing flexible and stretchable sensors. For instance, Lee et al.[67] reported a bioinspired highly sensitive piezoresistive composite sensor consisted of PU elastomer and sea-urchin shaped metal nanoparticle, as shown in Fig. 7a. Owing to the high aspect-ratio and high density of the structured long spikes, this composite sensor exhibited much higher sensitivity and faster response time than conventional spherical metal-filled composite

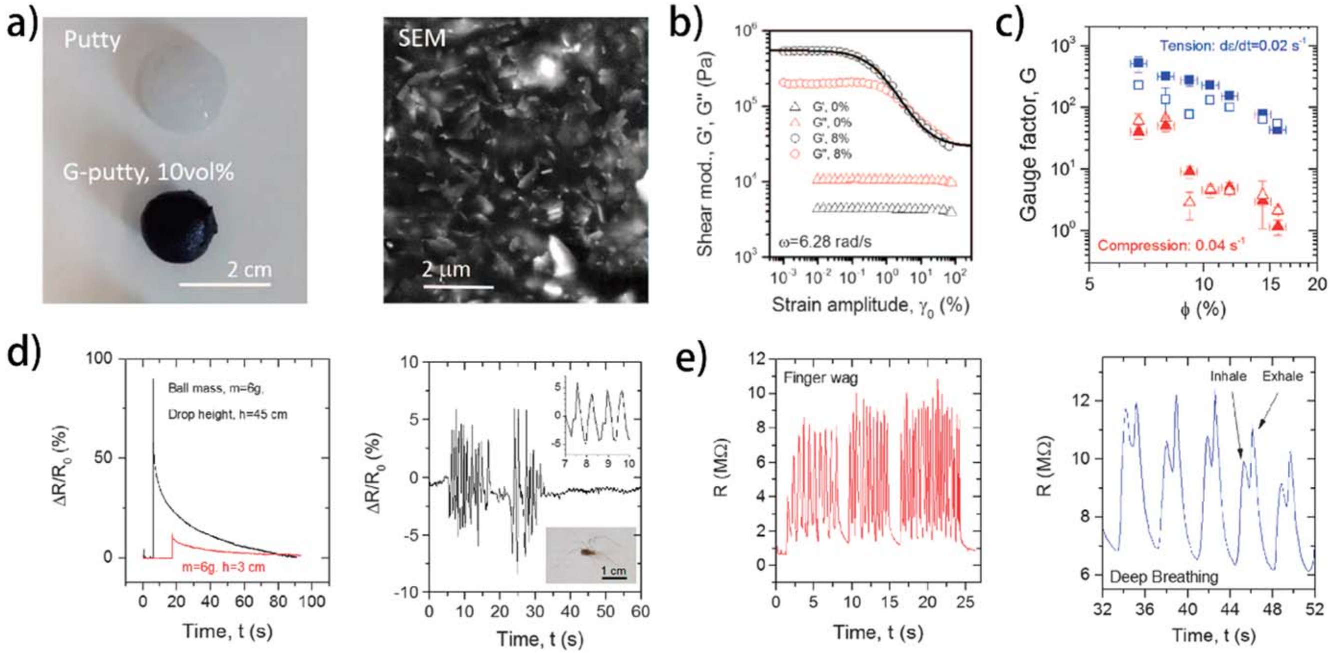

Figure 6. Graphene-based polymeric composite with highly viscoelastic Silly Putty matrix toward subtle pressure sensing applications. (a) Photograph of highly viscoelastic pure Silly Putty and graphene/Putty composite, and the SEM image of the surface of the graphene/Putty composite; (b) The rheological properties of the graphene/Putty composite; (c) The piezoresistive sensitivity (Gauge factor) of the graphene/Putty composite vs volume fraction of graphene fillers; (d) Graphene/Putty composite sensor used to detect subtle pressure including static weight-loading and dynamic footsteps of a small spider; (e) Demonstrations of graphene/Putty composite sensors for wearable electronic sensing applications.[105]

ones. Its outstanding piezoresistive performance enables the promising potential applications in wearable sensors. And, Gray[127] reported polymer nanocomposites by embedding various nanoparticles including Ni, Ag, and CNT into a polymer matrix. With nanoparticles embedded in PDMS, the composites reached good flexibility and Young's Modulus of 6.2 MPa with 55 wt% of Ni and exhibited some degree of piezoresistivity. Compared to rigid 0D metallic particles, 1D metal nanowires possess better mechanical flexibility and electrical conductivity, Ho et al.[123] utilized a simple solution-processable method to embed Ag nanowires and Au nanowires within flexible PDMS polymer (Fig. 7b). Due to the percolating Ag and Au nanowire networks, the composite showed very high sensitivity with a strain gauge factor of 236.6, which was applied in detecting human facial muscle movement activities. Besides, Wang et al.[128] reported multi-functional e-skin with three-sublayer structure with interpenetrating networks of Ag nanowires and the azobenzene buried between silk fibroin (SF) film and PDMS film. The e-skin exhibited high flexibility with elongation at break of 65% and the elastic modulus of 0.87 MPa. It also showed light-sensitivity and low resistivity of 1.3 Ω/sq. Moreover, from the inherent flexibility and nontoxicity, the conductive elastic components (such as conductive polymers[124,125] and conductive natural elastic materials[126]) have also been considered as other promising alternative conductive fillers for stretchable composite sensors. For instance, Wang et al.[126] decorated the natural elastic sunflower pollen microcapsules with CNTs for its electrical conductivity. Then, the conductive microcapsules were mixed with PDMS matrix to form piezoresistive composite sensors (Fig. 7c); the reported composite sensor achieved appropriate piezoresistive performance with a very low detection limit of 1.6 Pa and could accurately discriminate different spatiotemporal tactile stimuli. In addition, doped microcrystalline silicon also illustrated piezoresistive properties.[129] Garcia-Castro et al.[130] developed microsensors for pulse measurement by utilizing microcrystalline silicon fabricated on Kapton (polyimide film) via plasma enhanced vapor deposition. The microsensors exhibited high sensitivity with GF of approximately 100.

Conductive Foam-Based Sensors

Another approach to realize the conductive pathway variation is to make porous conductive materials. Numerous conductive foams have been proposed to make piezoresistive sensors for wearable applications.[131–133] Owing to the 3D interconnected structures, the conductive foam-based piezoresistive sensors possess many advantageous features, including large surface area, light weight, high flexibility. In this section, we divide these porous piezoresistive materials into four categories—monolithic conductive foams, conductive composite foams, conductive material-coated foams, and porous fibers based on their composition characteristics.

Monolithic conductive foams.—Monolithic porous conductive material is a 3D porous material made of a single conductive material such as CNT,[134–136] graphene,[137–140] and other carbonized conductive materials.[68,141] Both CNT and graphene are carbon-based conductive materials, which can be self-organized into 3D interconnected pores in varied sizes, amounts, and morphologies. Compared with the bulk carbon materials, monolithic CNTs or graphene foams have significantly increased surface area and reduced weight due to the interconnected 3D porous structures. This gives a broader possibility in tuning the electrical and mechanical properties of the foams, leading to extensive interests for advancing lightweight electronic applications, especially for electromechanical sensors.[142] For instance, Wang et al.[135] developed an ultra-lightweight (density $\sim$4 mg cm^{-3}) carbon foam based on joint-welded CNTs with mobile nanotube components and fixed nodes (Fig. 8a). The as-prepared monolithic CNTs displayed a promising piezoresistive response performance and excellent elastic recoverability under both mechanical compressive and tensile deformation. The piezoresistive response of the as-fabricated sponge was very stable under 1000 cycles loading of 25% tensile strain and 95% compressive strain. Apart from monolithic CNT foam, Ma et al.[139] developed a high-temperature chemical vapor deposition (CVD) method to fabricate 3D graphene foam for strain sensors using copper as the sacrificial template (Fig. 8b). The integrated

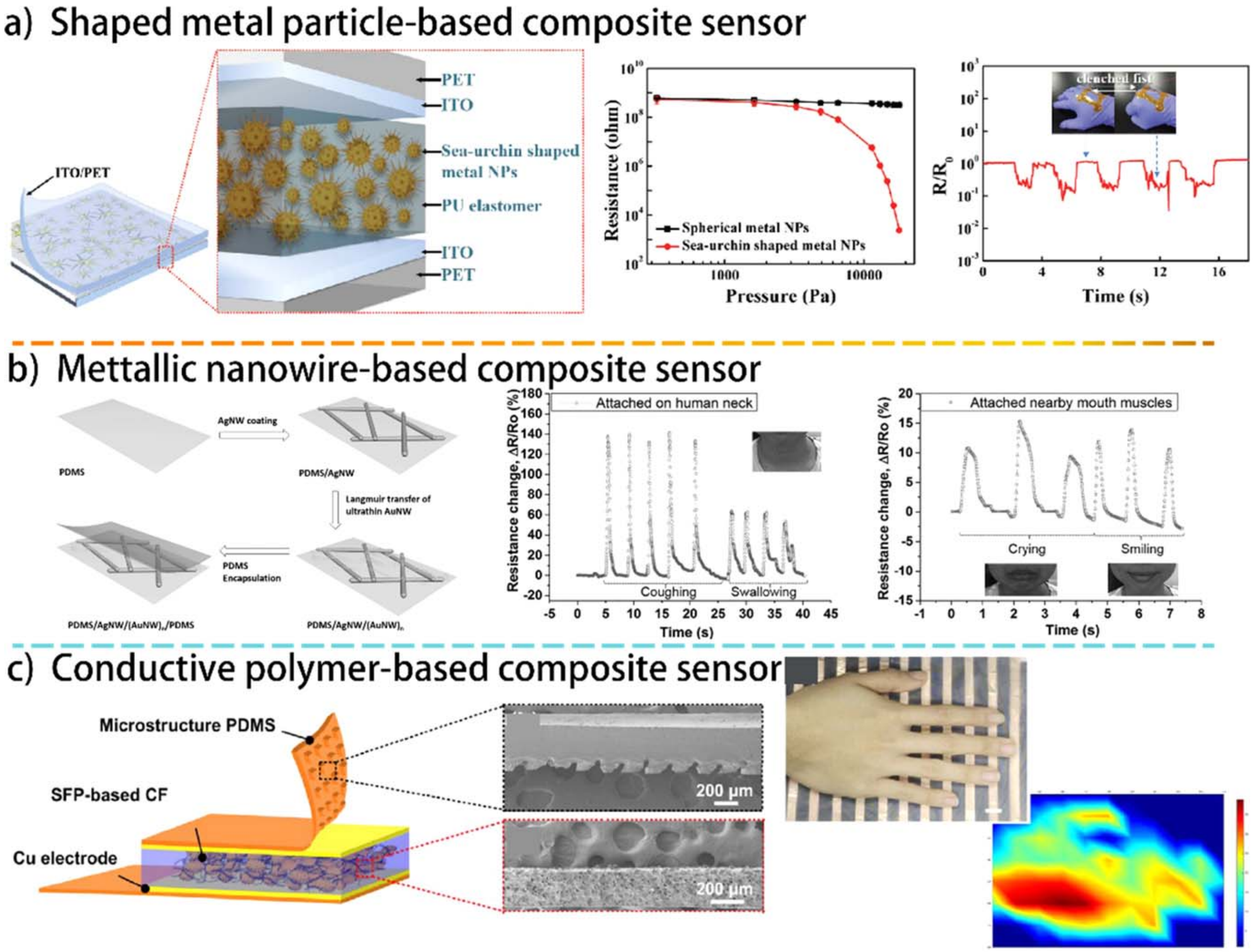

Figure 7. Other conductive material-based composites for advanced flexible and stretchable piezoresistive sensors. (a) Schematic illustration of the composite filled with sea-urchin shaped metal nanoparticles for wearable sensor applications.[67] Copyright 2016, John Wiley and Sons. (b) Schematic of the fabrication process of the transparent flexible hybrid Ag nanowire-Au nanowire/PDMS composite sensor, which could be "invisible" when attached to a human skin for small muscle movement detection.[123] Copyright 2017, John Wiley and Sons. (c) The schematic illustration and SEM images of the structure of the composite sensor consisting of conductive elastic microcapsule fillers and PDMS matrix, and its application in mapping the local pressure distribution of a human hand loading.[126] Copyright 2017, Elsevier.

highly conductive inner graphene sheet guaranteed the piezoresistive sensitivity of this foam structure and the electromechanical performance remained stable after one hundred cyclic loadings. The sensitivity up to 11.47 Pa^{-1} and ultra-low density down to $\sim$1.19 mg cm^{-3} enabled its potential application in imperceptible wearable electronic devices. However, due to the bundling phenomenon of CNTs and graphene sheets inside the porous structure, the carbon foam branches are rigid and brittle.[142] Under mechanical loadings, these branches undergo plastic deformation resulting in weak structural recoverability. The drawback restricts the practical usage of monolithic carbon foam in flexible electronics. To overcome this limitation and achieve good elasticity, the monolithic carbon foams were impregnated with elastic polymer as 3D-carbon/polymer composite.[115,116,143,144] Another alternative approach is to use nanowires or fibers as the collaborative support materials for the 3D carbon foam structure.[145] For example, Huang et al.[146] vertically grew environmentally stable polyaniline nanowires on the graphene sheets to form 3D porous structure (Fig. 8c). Due to the interconnections of the 1D nanowires and 2D sheets, the as-demonstrated collaborative monolithic graphene foam exhibited both high mechanical resiliency and good piezoresistive sensitivity ($\sim$0.77 kPa^{-1}).

The monolithic carbonized foam uses a foam material as a template followed by a carbonization step to make it electrically conductive.[147] Benefitting from the diverse mechanical properties of the selected template foams, the corresponding carbonized monolithic foam can be designed with desired features. For instance, Liu et al.[68] demonstrated a flexible and elastic sensor by carbonizing environment-friendly melamine foams (Fig. 8d). Due to the prominent elastic properties of this organic polymer and electric conductivity of the carbon, the as-prepared carbonized melamine foam displayed ultrahigh piezoresistive sensitivity ($\sim$100 kPa^{-1}) with outstanding reproducible sensing performance up to 11,000 cycles. Additionally, Hu group demonstrated that low cost and abundant natural wood could be processed into a high-performance structural material.[148] They converted wood into a highly compressible conductive sponge by carbonization method.[141] The as-fabricated foam exhibited compressibility up to 80%, high fatigue resistance of 10,000 mechanical loading cycles at 50% compressive strain, and good piezoresistive sensitivity suitable for potential application in human motion detection.

Conductive composite foams.—Different from the monolithic conductive foam, conductive composite foam refers to the 3D porous structure prepared by the composite material combining

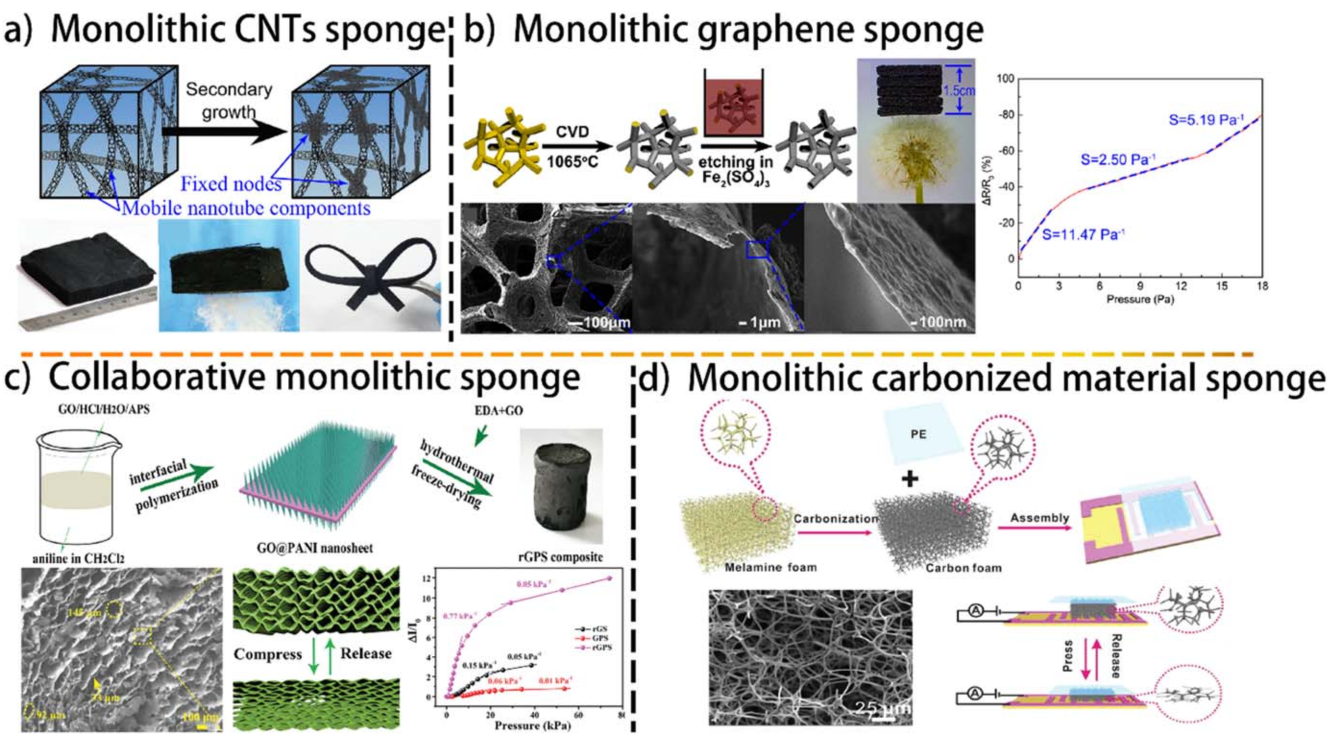

Figure 8. Monolithic conductive foams for advanced flexible and stretchable piezoresistive sensors. (a) Schematic diagram of CNTs welded by the amorphous carbon as the fixed nodes and the real images of the monolithic CNT foam standing on cotton and the tied bowknot of the foam.[135] Copyright 2017, John Wiley and Sons. (b) Schematic illustration of preparation processes using a copper sacrificial template and the corresponding SEM images of the monolithic graphene foam with a pressure sensitivity up to 11.47 Pa^{-1}.[139] Copyright 2017, American Chemical Society. (c) The fabrication processes and the SEM image of highly sensitive collaborative monolithic foam based on PANI nanoarrays grown on graphene sheets.[146] Copyright 2019, Royal Society of Chemistry. (d) The fabrication process, a zoom-in SEM image and the sensing mechanism of the monolithic carbonized foam using melamine foam as the template.[68] Copyright 2018, American Chemical Society.

polymeric components and conductive fillers. Generally, conductive composite foams can be fabricated via "casting-etching" and "freeze-drying" methods.[149,150]

The "casting-etching" process utilizes sacrificial materials as the temporary framework to assist the formation of 3D porous structures. Conventionally, easily accessible and environment-friendly sugar and starch are the most widely used sacrificial materials for this fabrication process. For instance, Wu et al.[151] utilized the carbon nanofiber (CNF)-coated sugar particles as the templates for the CNF/PDMS composite foam. After a warm water etching process to remove the sugar particles, the CNFs were partially embedded in the PDMS pore surface. Under compressive loading, the pores were condensed that led to the formation of the conduction pathways by the connected CNF networks, resulting in resistance change. The 3D microstructure provided the CNF/PDMS composite with good electromechanical sensitivity (gauge factor ∼6.5), linear response, and durability up to 70% strain. Additionally, ZnO[152] or Ni scaffold[153] and aqueous emulsion[154] are also used as sacrificial templates for the conductive foam composites. However, the enhanced sensitivity of these composite foams was limited by their "large" microscale pores. Under a specific porosity, the surface area of pores can be dramatically increased by reducing the pore size, leading to the huge increase of the conductive pathways when the pores are condensed. Based on this hypothesis, Li et al.[155] proposed that the sensitivity of the composite foams could be further enhanced by the nanoscale pores. They developed an elastic CNT/PDMS composite foam with nanoscale pores for tactile pressure sensing by casting-etching method using ZnO sacrificial nanoparticles (Fig. 9a). They found that the fully embedded CNTs were partially exposed to the porous surface, contributing to the conductive pathway variation when the composite was deformed. The as-fabricated nanoporous composite foam showed ultrahigh piezoresistive sensing performance with a strain gauge factor up to 300 and was able to detect subtle pressure down to 1 Pa with ∼70 ms fast response time. The paper has also demonstrated its practical applications in detecting both static water droplet loading and dynamic footsteps of a small cockroach movement.

The "Freeze-drying" is a thermally induced phase separation technique, which is also widely used to fabricate porous structures. For example, Huang et al.[156] reported a lightweight (density $< 0.123\ g\ cm^{-3}$) and flexible CNT/PU composite foam with aligned porous structures using directional freeze-drying method, as shown in Fig. 9b. The CNTs were first well dispersed in a solvent, then the PU particles were completely dissolved in this suspension followed by unidirectional freezing process to form aligned structure. After sublimation and drying processes, the CNT/PU foam was achieved. Owing to the aligned structural pores, the as-fabricated sample exhibited 30.9% higher compression strength than unaligned porous CNT/PU composites, as well as excellent piezoresistive sensitivity and reproducibility. Specifically, this composite sensor displayed an outstanding linear characteristic in the compressive strain range of 0%–77%. Liu et al.[21] also demonstrated a conductive graphene/PU composite foam with interconnected porous structure by freeze-drying. Compared with the conventional CNT/PU composite foam, the 2D graphene sheet fillers would effectively increase the pore wall thickness to form a robust porous structure with prominent mechanical recoverability and stable piezoresistive performance up to 90% compressive strain. Besides, cellulose foams made of interconnected plates networks can also be fabricated via the freeze-drying method. Owing to the spatial configuration of solids and voids, the cellulose foams not only possess ultra-lightweight and excellent mechanical elasticity, but also have good electrical conductivity and ultra-fast piezoresistive response.[69,159,160] Importantly, the cellular microstructures can be tailored by varying the concentration of the conductive suspension and freezing temperature, leading to the easy adjustable piezoresistive sensitivity, as shown in Fig. 9c.[157]

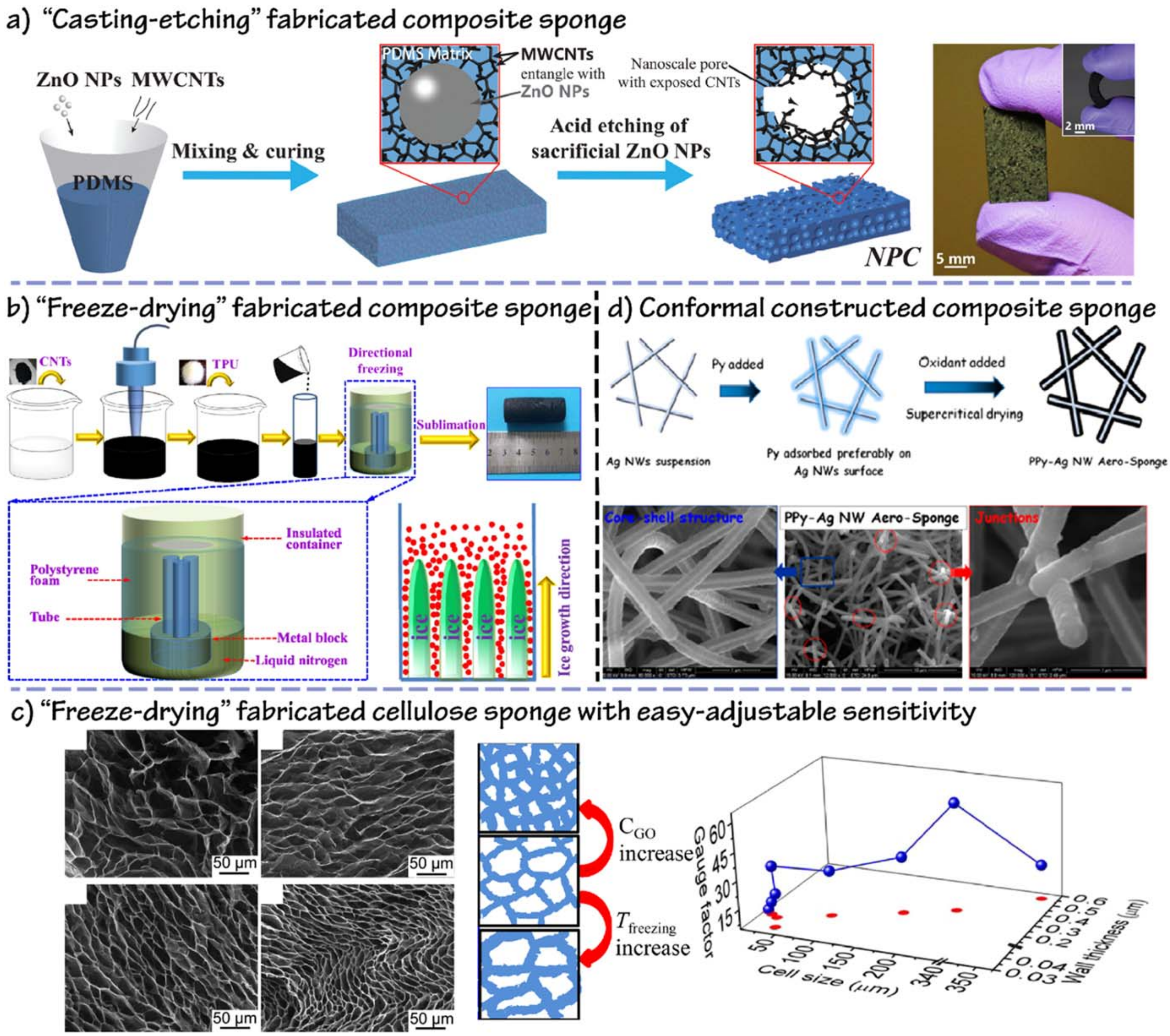

Figure 9. Conductive composite foams for flexible and stretchable piezoresistive sensors. (a) Schematic diagram of "casting-etching" process of the CNT/PDMS composite-based nanoporous foam using ZnO nanoparticles as the sacrificial material, and the real image of the as-prepared nanoporous CNT/PDMS composite.[155] Copyright 2019, Royal Society of Chemistry. (b) The schematic representation of the "freeze-drying" fabrication process of the CNT/PU composite foam for piezoresistive sensing application.[156] Copyright 2017, American Chemical Society. (c) The SEM images of the graphene/PDMS composite cellulose foam with tunable microstructure parameters and easy adjustable piezoresistive sensitivity by "freeze-drying" process.[157] Copyright 2016, American Chemical Society. (d) The schematic illustration and the corresponding SEM images of formation process of the conformally constructed Ag nanowire/PPy composite foam.[158] Copyright 2015, American Chemical Society.

Other nanomaterial assembly techniques were also demonstrated for making composite foams. For instance, He et al.[158] demonstrated an "incipient network conformal growth" method to fabricate a self-temperature-compensated composite foam for piezoresistive sensing applications. As shown in Fig. 9d, they first used silver nanowires to form an incipient network in H_2O-ethanol solvent followed by wet chemical coating of pyrrole monomer. After that, the 3D porous networks were constructed by supercritical CO_2 drying process. This Ag nanowire/polypyrrole composite foam sensor displayed a temperature-independent coefficient with good piezoresistive sensitivity of 0.33 kPa^{-1}, ultrafast response time ($\sim$1 ms), and promising sensing stability.

Conductive material-coated foams.—Conductive material-coated foams refer to materials that have pore surface of the readily available template decorated with conductive materials by coating techniques (such as solution dip-coating,[161] sputtering,[162] and wet-chemical deposition[163]). It is a straightforward way to make flexible foams with good electrical conductivity for various electronic applications.

Due to the fast and scalable features, solution dip-coating method has been frequently used to fabricate conductive material-coated foams. For instance, Yao et al.[75] reported a graphene-coated PU foam for piezoresistive sensing applications via the solution dip-coating method, as shown in Fig. 10a. They first dispersed graphene nanosheets in a solution, then dipped the polymer foam template in the prepared suspension. After centrifugation and drying processes, the graphene-coated PU foam was obtained. When a pressure was applied to this foam, the coated conductive graphene networks would make contact with each other, leading to the change of the electrical resistance. Similarly, Asaro et al.[164] reported an ultra-lightweight (density $\sim$ 0.13 g cm^{-3}) carbon black (CB)-coated

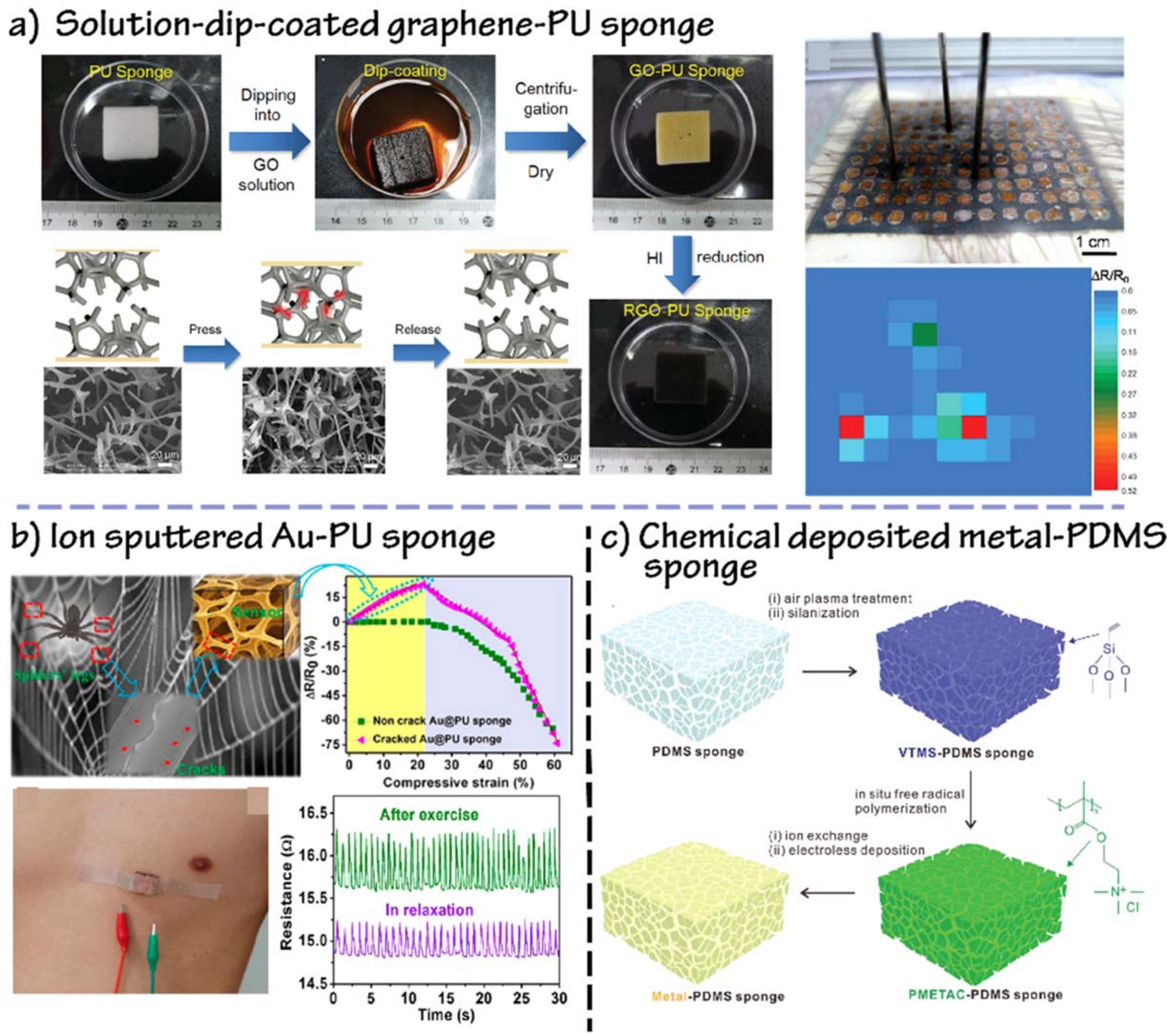

Figure 10. Conductive material-coated foams for flexible and stretchable piezoresistive sensors. (a) Schematic diagrams of the fabrication process based on solution-dip-coating and sensing mechanism of the graphene-coated PU foam, and its application in local pressure detection.[75] Copyright 2013, John Wiley and Sons. (b) The schematic representation of the gold ion-sputtered PU foam with spider-inspired crack channels and its application in human heartbeat monitoring.[162] Copyright 2017, American Chemical Society. (c) The schematic illustration of the formation process of the metal-coated PDMS foam by a wet-chemical deposition method.[173] Copyright 2016, John Wiley and Sons.

PDMS foam with promising piezoresistive sensitivity, reproducibility, and mechanical durability. Wu et al.[165] and Tewari et al.[166] also demonstrated a carbon nanofiber-coated PDMS foam and a CNT-coated PU foam for piezoresistive sensing applications, respectively. Apart from carbon materials, hydrophilic MXene,[167] conductive PEDOT:PSS polymer,[168] metal particle/nanowires,[169,170] or hybrid conductive materials[166,171] are also considered as promising alternative coating materials for non-conductive polymer foam templates. In addition, to achieve reliable adhesion between the conductive coating materials and the foam template, Guo et al.[172] pretreated the non-conductive polymer foam by O_2 plasma to increase the hydrophilicity of the pore surface for supramolecular coating assembly.

Besides the commonly used dip-coating method, sputtering and wet-chemical deposition are also considered as efficient ways to decorate the foam surface with conductive materials. For example, Wu et al.[162] directly coated metallic gold (Au) to a commercial PU foam by sputtering. To mimic the crack shapes on spider's feet, they created many crack channels on the coated Au lamina to improve the piezoresistive performance of an Au-PU foam (Fig. 10b). The as-fabricated sensors displayed good sensitivity (up to 96 Pa^{-1}), ultralow pressure detection limit (0.568 Pa), and ultrafast response time (9 ms), as well as excellent recoverability. Owing to these desirable electro-mechanical features, it could be utilized as wearable electronics for human health monitoring. Furthermore, Liang et al.[173] reported a wet-chemical deposition method to coat conductive metals to a PDMS foam, as shown in Fig. 10c. They first modified the PDMS foam surface with the poly[2-(methacryloyloxy) ethyl-trimethylammoniumchloride] (PMETAC) polymers by a radical polymerization step to increase its surface wettability, then the PMETAC-modified PDMS foam was used as the template for the electroless metal deposition process to form metal-coated foam. Due to the reliable adhesion of this wet-chemical deposition method, the as-fabricated conductive foam exhibited stable electrical conductivity and piezoresistive response under repeated cyclic deformation (up to 500 cycles).

Porous fibers.—Porous fibers refer to the piezoresistive materials consisting of conductive fibers with fibrous structure. Three-dimensional compliant fibrous structures could offer flexible or stretchable behaviors out of rigid conductive materials for sensing applications. Compared with two-dimensional structures that have drawback of relatively less deformation in thickness direction, three-dimensional fibrous structures can offer more prominent flexibility, longer durability, and higher sensitivity, owing to more significant compressive deformation along thickness direction.[77] Under external loading, the small compressive deformation causes microstructures to contact each other, resulting in more conductive pathways and more piezoresistive responses. In this case, many porous fibers have been developed for piezoresistive sensing applications,[174] such as yarn-like carbon fibers,[175,176] carbonaceous composite nanofibers,[177] and other electrospun conductive fibers.

For instance, Ryu et al.[178] reported an extremely elastic yarn-like carbon nanotube fiber (CNTF) piezoresistive sensor using dry-spun CNTs, as shown in Fig. 11a. Due to the internal fibrous structures of the self-assembled carbon nanotubes, the connection area of the CNTFs would be varied under mechanical loading, leading to the piezoresistive effect. As they grew the yarn-like CNTFs on the ultra-flexible Ecoflex under uniform stress distribution when the yarn was stretched, the as-demonstrated piezoresistive sensor could be stretched over 900% strain with satisfactory sensitivity for human motion detection. In addition, yarn-like graphene fibers were also demonstrated by Cheng et al.[179] for sensing tensile, bending, and torsion loadings.

Besides yarn-like carbon fibers, carbonaceous composite fibers are also very attractive for piezoresistive sensing applications. Wang et al.[182] reported a piezoresistive strain sensor fabricated from poly (styrene-butadiene-styrene) and few-layer graphene composite fiber. They used styrene-butadiene-styrene (SBS) as a matrix for conductive few-layer graphene (FLG), synthesizing graphene composite fiber. Due to remarkable electrical and mechanical performance of FLG and significant flexibility of SBS matrix, the SBS/FLG composite fiber sensor has several superior performances simultaneously such as high durability, remarkable sensitivity with gauge factor of 2546 at a strain of 100% and gauge factor of 160 at a strain of 50%, and significant stretchability with a failure strain range more than 110%. In addition, Si et al.[180] reported a honeycomb structured carbonaceous composite nanofiber by carbonizing the SiO_2 nanofiber with added konjac glucomannan powder for piezoresistive sensors (Fig. 11b). Benefiting from the high elasticity (compression strain up to 80%) and robust sensitivity ($\sim$1.02 kP^{-1}), the sensor could be used to detect human muscle movements.

Furthermore, fibrous structured piezoresistive sensors can be constructed by self-assembly of other conductive electrospun fibers. For instance, Zhao et al.[183] developed a sandwich-structured piezoresistive pressure sensor with electrospun nanofiber mats, which has a large surface area and significant porosity. As supporting, sensing, and packaging layers, several layers of PLA–SF–COL mat and PPy-coated mat were packed, constructing piezoresistive pressure sensor with sandwich structure (Fig. 11c). In addition, Kweon et al.[181] reported a pressure sensor based on electrospun conductive nanofibers with three-dimensional structure. They fabricated multi-array piezoresistive pressure sensors using three-dimensional electrospun conductive nanofibers to construct wearable devices.

Architected Conductive Materials

To achieve higher sensitivity, geometry effects of architecture design have been incorporated into sensor development in addition to material development. With designed structures that could amplify mechanical loading effects, the resulting resistance change

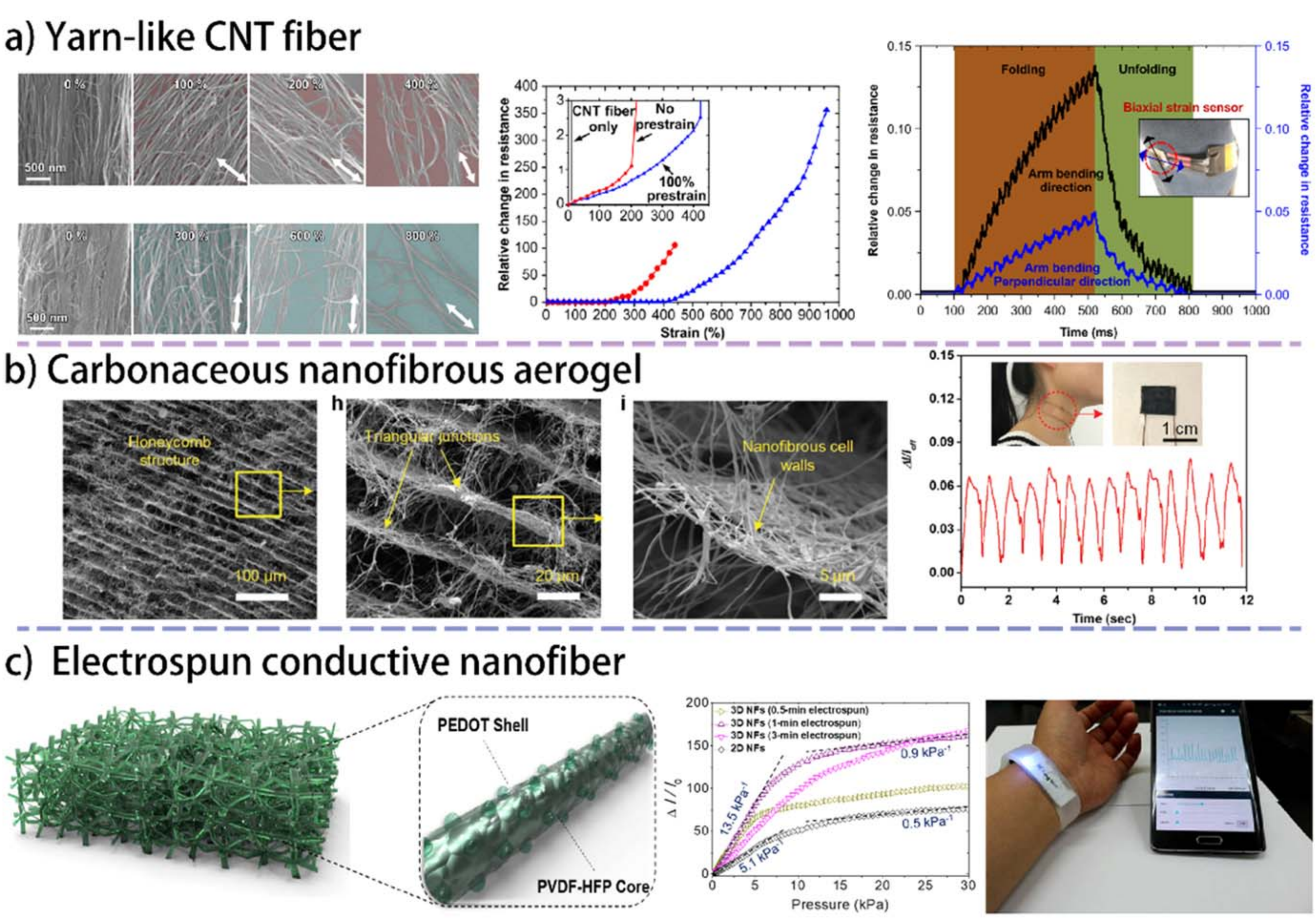

Figure 11. Porous fiber-based flexible and stretchable piezoresistive sensors. (a) The SEM images and electromechanical characterization of yarn-like CNTFs for various strains, and its applications in human motion monitoring.[178] Copyright 2015, American Chemical Society. (b) SEM images of the carbonaceous nanofibrous composite with porous honeycomb structure, and its application in human muscle movements detection.[180] Copyright 2016, John Wiley and Sons. (c) Schematic illustration of electrospun 3D nanostructured PVDF-HFP/PEDOT nanofiber mats and HR-TEM images of PVDF-HFP/PEDOT nanofibers deposited with different oxidant concentrations and reaction times.[181] Copyright 2018, Nature Publishing Group.

in the material system can be enlarged and lead to a better sensitivity. The design of the structures may either be nature-inspired, periodic arrays, or hierarchical combination of architecture and additives, as summarized in the following subsections.[184–186]

Nature-inspired architectures.—Living organisms have developed delicate biological systems to sense the mechanical signals in nature. For example, mammalian have cochlear hairs that could be easily distorted upon small vibration to sense sound.[187] Inspired by the design, Suh group[9,188] developed a sensor system with two arrays of Pt-coated polymer nanofibers on PDMS substrates (Fig. 12a). When a small pressure is applied, the upper and lower layer of nanofibers contact and pair with each other by van der Waals force. The distorted geometry could then be converted into resistance change, which can be detected by external circuits. The sensor is reported to be able to detect a normal pressure down to $\sim$5 Pa with less than 50 ms delay time. Furthermore, as shown in Fig. 12a, shear and torsion loadings could trigger different deformation modes, hence the sensor could also detect other mechanical loads.

As another example, the interlocked epidermal-dermal layers beneath our finger-tip skins provide the recognition of contact force.[192] Inspired by the architecture, Park et al.[193] fabricated interlocked microdome arrays of PDMS-CNT composite as shown in Fig. 12b. Upon external pressure, the concentrated stress at dome-dome contact point enlarges the contact area as well as the tunneling currents, which provides a high sensitivity of $\sim$15.1 kPa^{-1} and a fast response time of 40 ms. Similar to the ear structure, by arranging the microdome hexagonally, the sensor also has capability of differentiating shear and bending.[189] Additionally, by applying the same architecture to ferroelectric materials, this piezoresistive pressure sensor could be coupled with a temperature sensing function, which is even closer to the capabilities of our skin.[194] Other researchers have also been interested in this architecture. Wang et al.[195] used Ti_3C_2/natural microcapsule bio-composite films to exhibit excellent elastic modulus (0.73 MPa) as well as high pressure sensitivity (24.63 kPa^{-1}).

Other than human skins, the chameleon and cephalopod skins have extra color-changing abilities. Inspired by their abilities, Bao group combined the pressure sensing and color-changing functions

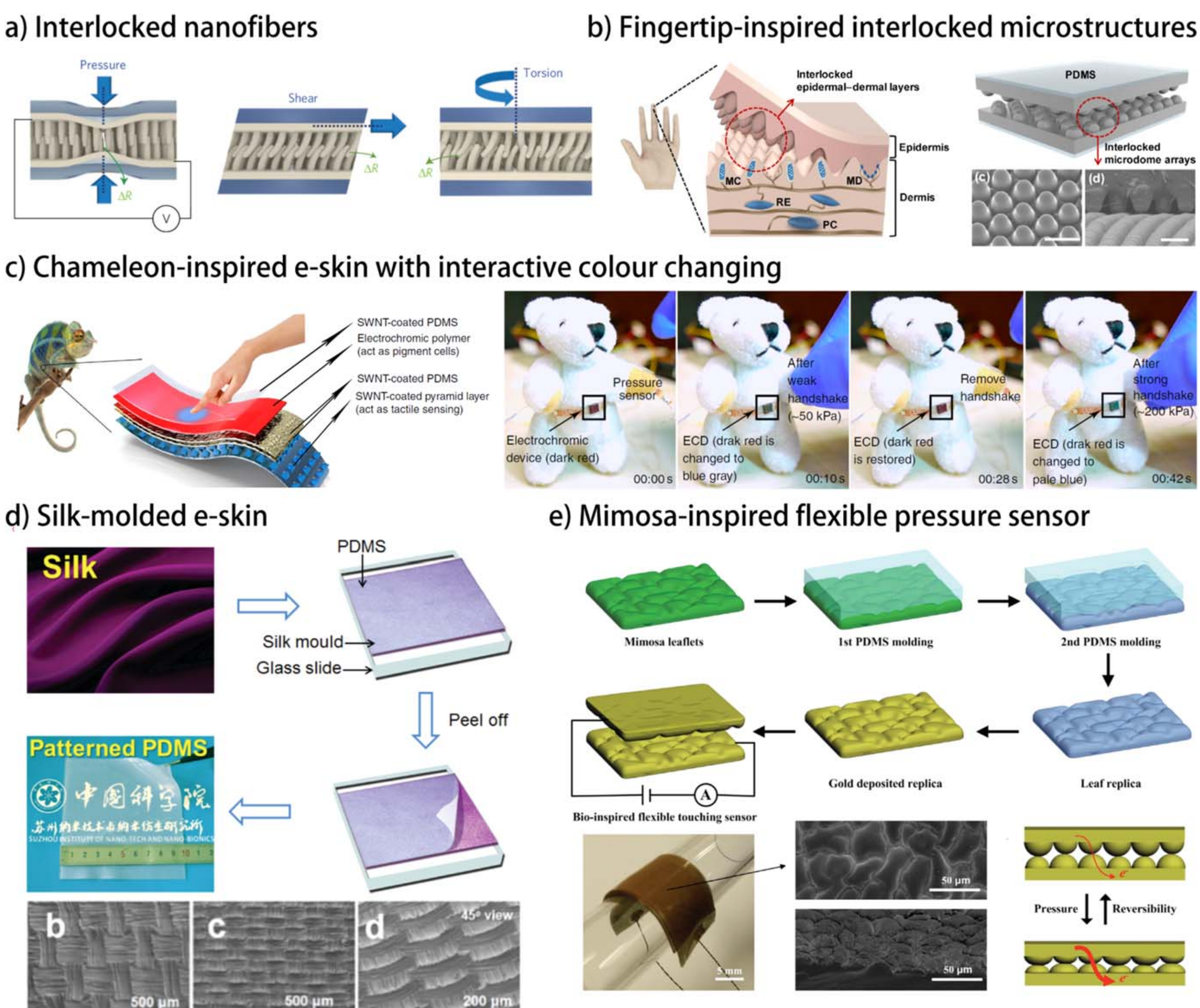

Figure 12. Piezoresistive sensors with nature-inspired architectures. (a) Schematic diagrams of the multi-directional sensing capability of the cochlear hair-inspired interlocked nanofiber arrays.[9] Copyright 2012, Nature Publishing Group. (b) The schematic representation and SEM images of the fingertip-inspired interlocked microstructures.[189] Copyright 2014, American Chemical Society. (c) The schematic illustration and color-changing experiments of the chameleon-inspired e-skin.[190] Copyright 2015, Nature Publishing Group. (d) The fabrication process and SEM image of the silk-molded e-skin.[191] Copyright 2014, John Wiley and Sons. (e) The replication process and SEM images of the Mimosa-inspired flexible pressure sensor.[33] Copyright 2015, John Wiley and Sons.

together on an electronic skin (e-skin) system.[190] As shown in Fig. 12c, the CNT-coated pyramid layer acts as a pressure sensor, which conveys the signal to electrochromic polymer to visually express the current pressure level, from dark red for no pressure to pale blue for strong pressure (~200 kPa).

However, fabricating the nanofibers and microstructures could be complex and costly. Thus, living creatures and their products were directly used as the molds to simplify the process. As shown in Fig. 12d, Wang et al.[191] replicated silk's microstructure on PDMS and CNT thin films. The sensing device exhibited good sensitivity (1.80 kPa^{-1}) and ultrafast response time (<10 ms) for sensing very low pressure down to 0.6 Pa. Applying a similar cost-effective molding method, Wei et al.[196] replicated rose petals with PDMS thin films and Cu-Ag nanowires. Rose petals have micropapillae on their surfaces, whose structures are similar to human epidermis and the feature size is also close to Cu-Ag nanowires. The e-skin not only showed good sensitivity (1.35 kPa^{-1}) and fast response time (~30 ms), but also showed superhydrophobic behavior, which is found in the original rose petals as well. Just like the petals, the superhydrophobicity can make the surface repel water and clean itself easily.

Within the kingdom Plantae, one of the most representative touch-sensing plants is *Mimosa*, which can close its leaves upon external stimulus. To mimic this behavior, Su et al.[33] used PDMS to mold the replica of Mimosa leaves and coat it with Ti and Au layers to make it conductive, as shown in Fig. 12e. Due to the existence of these protuberant microdomains, the sensor system has ultrahigh sensitivity of 50.17 kPa^{-1} and fast response time of 20 ms. More importantly, due to the nature of molding process, the fabrication of this sensor (as well as the previous molded system) is very cost-effective without the need of expensive equipment.

Periodic architectures.—Other than bio-inspired designs, pyramidal micro arrays have been employed in capacitive sensors due to the high sensitivity brought by the sharp tip.[16,197] This idea could be easily translated to piezoresistive sensors. Zhu et al.[198] fabricated a sensor consisting of reduced graphene oxide (rGO)/PDMS micro pyramid arrays and flat indium tin oxide (ITO)-coated PET films as Fig. 13a. This sensor is exceptionally good at <100 Pa pressure range sensing, with a good sensitivity of ~5.5 kPa^{-1} and an ultrafast response time of 0.2 ms. In the same year of 2014, Choong et al.[199] used conductive PEDOT:PSS and an aqueous polyurethane dispersion (PUD) elastomer blend to fabricate a pressure sensor based on micro-pyramid arrays. This sensor could maintain high performance (~10.3 kPa^{-1} sensitivity) at up to 40% elongation.

Since then, more materials and designs have been explored. Khalili et al.[204] prepared interlocked micropyramidal structures using CNT-PDMS composite. Similar to the previously mentioned interlocked nanofiber structures, the interlocking grants the sensor to detect loadings from multiple directions. In addition, Tian et al.[205] used graphene oxide (GO) and laser-scribed graphene (LSG) as materials to reach both good sensitivity (0.96 kPa^{-1}) and wide sensing range (0~50 kPa). Li group[206] paired Au-coated PDMS pyramid arrays with p-type organic semiconductor dinaphtho[2,3-b:2′,3′-f]thieno[3, 2-b]thiophene (DNTT) to realize an ultrahigh sensitivity of 514 kPa^{-1}. The same group has also used PDMS/polypyrrole (PPy) arrays over Au electrode coupled PET film, which is reported to exhibit near 2000 kPa^{-1} sensitivity when using a sharp geometry.[207] Using this mechanism, the highest sensitivity was reported by Huang et al.,[200] which claimed to have 8655.6 kPa^{-1} with CNT/PDMS composite pyramid arrays and ITO/PET film. To reach this sensitivity, a low-conductivity tip/high-conductivity body structure was employed by controlling the CNT distribution (Fig. 13b).

Besides pyramidal geometry, other architectures including pillars and domes have been studied. As shown in Fig. 13c, Shao et al.[70] used photolithography to fabricate Au covered micropillar arrays and could tune the sensitivity from 0.03 kPa^{-1} to 17 kPa^{-1} by varying gaps between the pillars. Lee et al.[201] made cylindrical structures with PEDOT:PSS coated electrospun polyether block amide (PEBA) film, as illustrated in Fig. 13d. Without complex micro-fabrication technology, the electrospinning technique of making the main sensing element is very fast and cost-effective. The sensitivity is also tunable by varying the fiber diameter, from 5.34 kPa^{-1} for 30 μm to 1.85 kPa^{-1} for 70 μm. For the spherical geometry, Zhong et al.[202] deposited PPy coated poly(vinyl alcohol-co-ethylene) (PVA-co-PE) nanofibers and elastic polyolefin elastomer (POE) nanofibers onto PDMS substrate (Fig. 13e). When pressure is applied, the dome-shaped 3D fiber network makes contact with another layer of micro dome arrays resulting in the change of the resistivity with a sensitivity of 1.24 kPa^{-1}.

For rational comparison between architectures, Peng et al.[208] used ITO coated PDMS to replicate multiple 3D-printed microstructure arrays: pyramid, semi-sphere and semi-cylinder with same feature sizes and gaps. The experiments showed that semi-cylinder microstructure had the best performance among the three candidates. However, to be noted here is the 3D-printed mold has very limited resolution and accuracy (~1 mm level), which could be a setback of this study. To address this issue, Park et al.[76] compared microdome, micropyramid, and micropillar arrays with a much higher fabrication precision, as shown in Fig. 13f. The results suggested that microdome structures have the best sensitivity for normal, tensile, and bending loads, while micropillar is best for detecting shear loads. And after all, interlocked microstructures are better than the combination of single array and planar films.

Beyond those additive architectures, the subtractive hollow-pillar structure could also work as a strain amplifier to increase sensitivity. Bao group used PDMS and CNT films with hollow-pillars to perform multi-directional sensing, as shown in Fig. 13g.[203] The result suggests both "positive" and "negative" micropillar arrays could work well in detecting multiple forms of mechanical loads.

Hierarchical architectures.—Based on the previously mentioned structures, a hierarchical combination of different architectures and additives could be a good way of designing novel high-performance piezoresistive sensors.

One of the most straightforward methods is attaching additional nanowires over microstructures. As Fig. 14a shows, Ha et al.[209] grew ZnO nanowires over PDMS micropillars, then coated them with Pt/Ni films (as ZnO nanowire arrays have very high resistance). The hierarchical structures were designed to be interlocked with each other so that both the contact and bending of ZnO nanowires could help providing a good sensitivity (6.8 kPa^{-1}) and ultrafast response time (<5 ms). As a lower cost alternative, Ma et al.[71] coated Ag nanowires over PDMS semi-cylinder arrays and the sensor exhibited 2.3 kPa^{-1} sensitivity. However, to get even better performance in directional sensing, directional depositing of nanowires is still needed. Most recently, Zhu et al.[63] grew vertically-aligned Au nanowires over PDMS micro pyramid arrays. The hierarchical sensor showed up to 23 kPa^{-1} sensitivity and a large area multi-axial pressure mapping was also demonstrated.

Besides adding nanowires, introducing pores to microstructures has been studied recently. As shown in Fig. 14b, Yang et al.[210] fabricated porous PDMS micro pyramid arrays using stacked sacrificial PS beads. With the sensitivity contributed by both pyramid and pore structures, the sensor's performance reached 449 kPa^{-1} in < 50 Pa pressure regime. Other than the previously mentioned microstructures, Wei et al.[214] used a herringbone structure made by CNT/thermoplastic polyurethane (TPU) foam to form the piezoresistive element. In addition, Wang et al.[215] developed a TPU/Ag conductive ink for direct ink writing-based 3D printing of flexible sensors, which have a good sensitivity (5.54 kPa^{-1}) across a wide measurement range (10 Pa to 800 kPa).

Next, another category of hierarchical structures is wrinkles. In 2012, Xu et al.[211] used prestrained PDMS substrate to create wavy ribbons of Au/Pd coated CNT (Fig. 14c). The results showed the potential of making stretchable conductors with the out-of-plane buckling or swelling effects. Then, Wei et al.[216] coated stretched PU

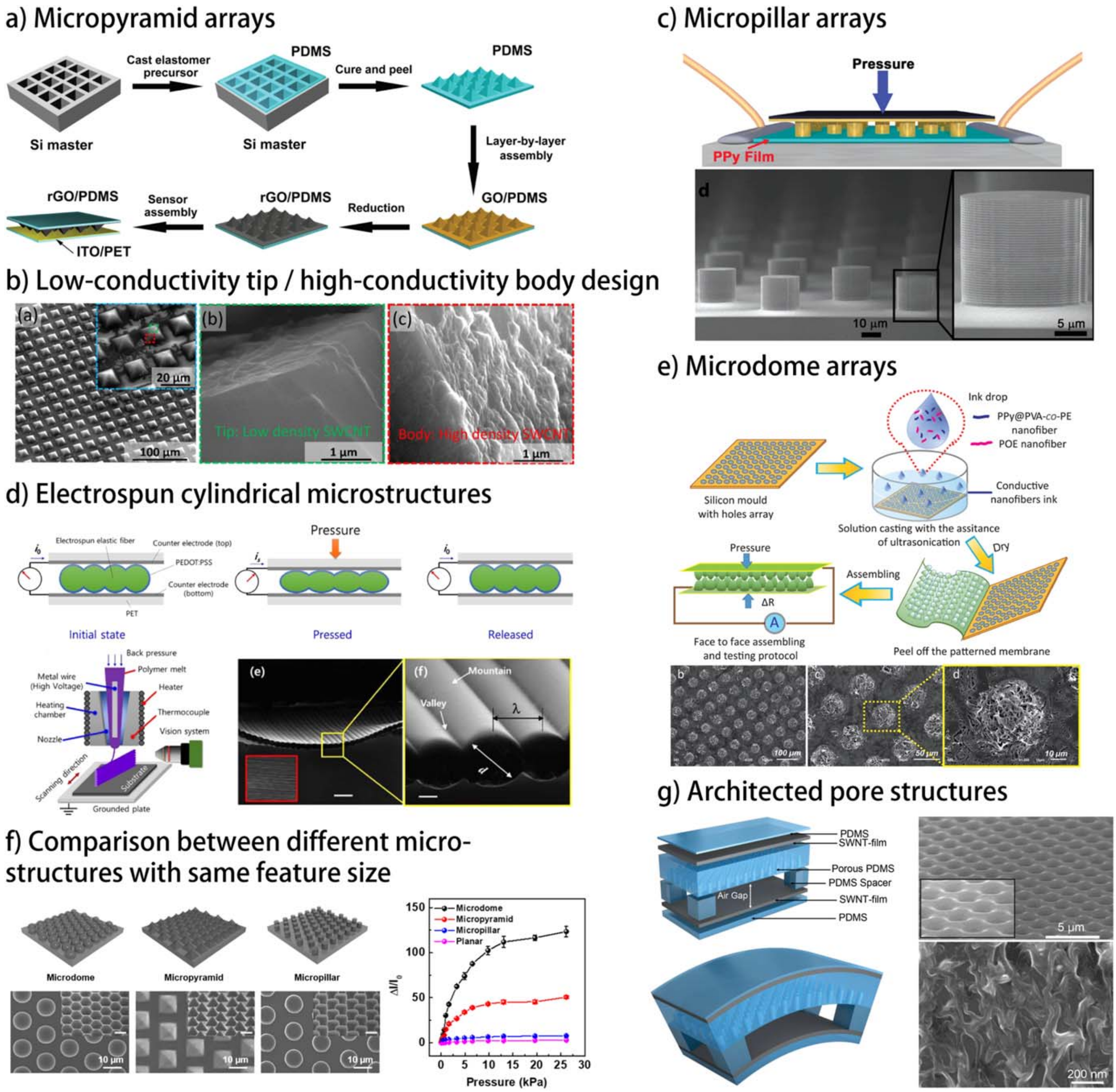

Figure 13. Piezoresistive sensors with periodic architectures. (a) Schematic diagrams of the fabrication process of micropyramid arrays.[198] Copyright 2014, John Wiley and Sons. (b) The SEM images of the low-conductivity tip/high-conductivity body design of micropyramid.[200] Copyright 2017, Elsevier. (c) The schematic illustration and SEM images of the micropillar arrays.[70] Copyright 2014, John Wiley and Sons. (d) The schematic representation, fabrication process and SEM images of the electrospun cylindrical microstructures.[201] Copyright 2018, IOP Publishing. (e) The fabrication process and SEM images of the microdome arrays.[202] Copyright 2016, Royal Society of Chemistry. (f) The SEM images of the different microstructures with same feature size and the current-pressure relationship for different architectures.[76] Copyright 2018, Nature Publishing Group. (g) The schematic diagrams and SEM images of the architected hollow-pillar structures.[203] Copyright 2014, John Wiley and Sons.

fibers with Ag nanowires to form fibers with wrinkled microstructures, which is sensitive to both normal pressure (0.12 kPa^{-1}) and bending deformations (0.012 Rad^{-1}). Instead of mechanical pre-strains, Gao et al.[212] utilized polymer swelling to form surface wrinkles over micro pillar arrays, which enlarged system conductivity change by three times, as shown in Fig. 14d. To form multiscale wrinkles over 3D surfaces, Mu et al.[213] applied blown film extrusion (a common method to make plastic films) to expand polyacrylic ester (PEA) films, then coated them with rGO solution to get both short and long period wrinkles, as illustrated in Fig. 14e. This film is transparent and could be stretched up to 400%, which is very versatile for piezoresistive applications. In addition, Bae et al.[217] used selective etching and thermal oxidation of Cu, and CVD growth of graphene to obtain a hierarchically patterned structure. After replicating it with PDMS, a micro dome array with rough surfaces was formed and showed a good sensitivity (8.5 kPa^{-1}) over a wide pressure range (up to 12 kPa). Recently, Yu et al.[218] used ultra-violet/ozone microengineering technique to fabricate wrinkled PDMS substrate with CNT arrays over its surface. This cost-effective method could be conducted at room temperature in an ambient environment, and the sensor offered a sensitivity of 0.1 kPa^{-1} in the range of 7 Pa to 50 kPa. Furthermore, Yang et al.[219]

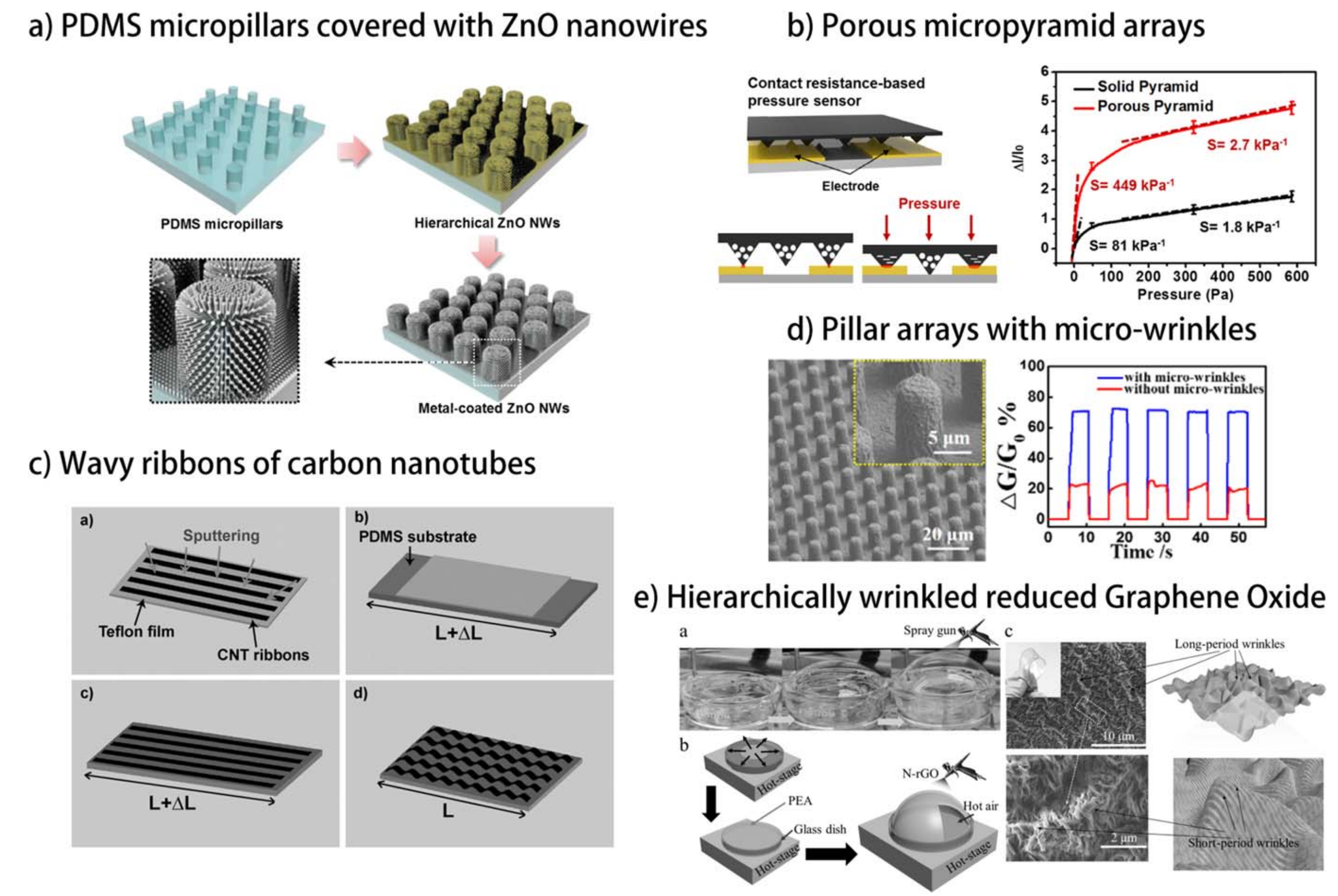

Figure 14. Piezoresistive sensors with hierarchical architectures. (a) Schematic diagrams of the fabrication process of PDMS micropillars covered with ZnO nanowires.[209] Copyright 2015, John Wiley and Sons. (b) The diagram of the micropyramids with hierarchical pores and the performance comparison between microstructures with and without pores.[210] Copyright 2019, American Chemical Society. (c) The fabrication process of wavy ribbons of CNT.[211] Copyright 2012, John Wiley and Sons. (d) The SEM images of the micropillar arrays covered with micro-wrinkles and the performance comparison between with and without micro-wrinkles.[212] Copyright 2016, American Chemical Society. (e) The fabrication process and SEM images of the hierarchically wrinkled reduced Graphene Oxide (rGO).[213] Copyright 2016, John Wiley and Sons.

made three-scale wrinkling of PPy films: the first two scales were formed during PPy film growth over compliant PDMS substrate and the third scale was generated by heating. The as-fabricated sensor showed a high sensitivity of 19.32 kPa^{-1} and a low detection limit of 1 Pa. Overall, the coupling of different scales of structures, pores and additives suggests a promising way for combining the advantage of each sensor design and improving their performances.

Finally, textiles are also considered as fibrous materials with hierarchical structures, derived from several levels of integration. Fibers, as the basic unit with a significant ratio of length to diameter, are interlaced to construct thread, which is the first integration. Then, in the second level of integration, threads turned into yarns via being twisted. In the third level of integration, yarns form textiles through various techniques including knitting and weaving.[220] In terms of higher hierarchical level, lots of different materials or composites are fabricated onto textile structures to achieve various kinds of functionality.[221] Conductive materials such as carbon nanotube (CNT),[222,223] graphene,[224] graphene/polymer nanocomposites, and other conductive polymeric composite materials[225–227] are incorporated on textile structure for piezoresistive sensors.

As one of the most popular conductive materials, carbonized materials such as carbon nanotube (CNT) could be patterned on a textile structure as a piezoresistive sensor. For instance, Liu et al.[36] demonstrated an all textile-based pressure sensor composed of an interdigitated textile electrode at bottom and bridge of CNT fabric on top (Fig. 15a). The resulting pressure sensor has a large area sensor arrays and showed a high sensitivity of 14.4 kPa^{-1}, mechanical stability with 1000 cycles, low detection limit of 2 Pa, fast response time of ∼24 ms, and low power consumption of less than 6 μW. Thus, according to these merits, the textile sensor could be utilized in wearable devices for monitoring human motions such as hand gestures and physiological signals as real-time pulse waves. In addition, Deignan et al.[223] reported the textile-based piezoresistive sensors constructed with carbon loaded conductive yarns for the application of diagnosis of spine diseases and arthritis, in the Modified Schober's test, which is a standard clinical test for measuring the flexion of the spine.

Besides CNT, graphene is another conductive material popular in piezoresistive sensing. Yang et al.[224] demonstrated a close-fitting and wearable strain sensor by utilizing graphene textile which is free from polymer encapsulation (Fig. 15b). Due to the outstanding performance of graphene oxide, graphene textile strain sensors demonstrated significant gauge factors as the resistance decreased distinctively while a strain increased. The graphene textile strain sensor exhibited great potential for wearable devices due to its sensitivity with maximum gauge factor of ∼26 with an 8% strain range at y direction and of ∼1.7 with a 15% strain range at x direction, long-term stability, and remarkable comfort due to close-fitting with the human body.

Moreover, metal materials including Ag nanoparticles and metal nanowires could also be patterned on textile substrates to fabricate piezoresistive sensors. For instance, Gao et al.[65] demonstrated

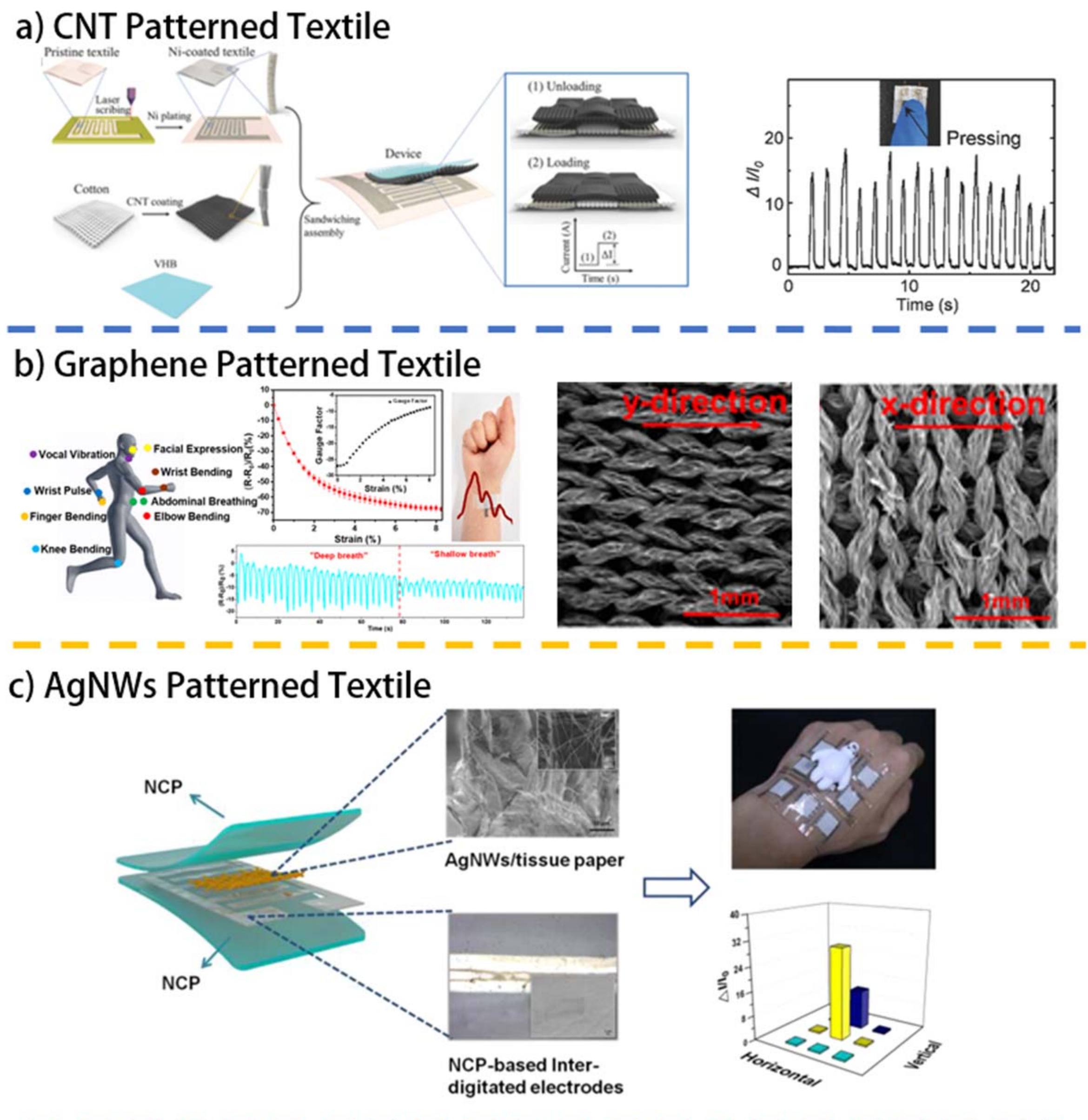

Figure 15. Textile-based flexible and stretchable piezoresistive sensors. (a) The fabrication of CNT patterned textile-based pressure sensors, a photograph image and current signal response to dynamic mechanical forces of pressing.[36] Copyright 2017, John Wiley and Sons. (b) Schematic diagram of characterization and application of graphene textile strain sensors and SEM images of the graphene textile in the x- and y-directions.[224] Copyright 2018, American Chemical Society. (c) Schematic illustration of the fabrication, characterization, and application of all paper-based piezoresistive pressure sensors with AgNWs.[65] Copyright 2019, American Chemical Society.

piezoresistive pressure sensors based on paper tissue coated with silver nanowires (AgNWs) via a facile, low cost, and environment-friendly approach (Fig. 15c). With good sensitivity of 1.5 kPa $^{-1}$ and low cost, the all paper-based piezoresistive (APBP) pressure sensor could be utilized as soft electronic skin to monitor physiological signals. In addition, Zhang et al.[225] reported a textile-supported piezoresistive pressure sensor applied to human vital sign monitoring. They used pre-cut cohesive thermoplastic to assist the patterning and assembly process of the piezoresistive pressure sensor, enabling the sensor highly sensitivity, good responding speed (400 ms under a pressure of 1.0 kPa) and remarkable durability of over 500 cycles of pressure loading.

For conductive polymeric composite materials, Lee et al.[226] fabricated ultrasensitive textile pressure sensors by coating styrene-butadien-styrene (SBS) polymer on the surface of Kevlar fiber with Ag nanoparticles converted into SBS. Via stacking the conductive fibers with PDMS dielectric layers perpendicular to each other, textile pressure sensors were fabricated with excellent stability for more than 1000 cycles, good sensitivity of 0.21 kPa^{-1}, and fast response time of tens of millisecond range (∼40 ms).

Summary and Perspectives

Due to the extensive studies in the past decade, remarkable progress has been made for the design and fabrication of high performance piezoresistive sensors possessing desired high sensitivity and stretchability. In this paper, we have comprehensively reviewed the recent progress in flexible and stretchable piezoresistive sensors and their applications. The primary approaches applied to construct piezoresistive sensors with a combination of mechanical conformability and electrical sensitivity are highlighted first. Then, based on their material composition and structural characteristics, we categorized these newly emerged material/structure strategies into three types: conductive polymeric composite, porous conductive material, and architected conductive material. The detailed fabrication methods and electromechanical performances and applications of each type of piezoresistive sensors are discussed subsequently. There have been many reports that demonstrated flexible and stretchable piezoresistive sensors with high sensitivity, low detection limit, fast response time, and excellent stretchability, which enable these sensors to be an indispensable part of future wearable electronics for intelligent human-machine interfaces. In addition, soft sensors can be beneficial for environment with large pressure such as underwater because they can withstand high pressures due to the incompressible nature of the matrix material.

In terms of the fabrication method, one of the mostly used approaches is forming composites by adding commercially available nanofillers to the flexible matrix materials. This is generally a low cost method to make flexible piezoresistive sensors. Based on different selections of nanofillers, matrix materials, and their mass ratios, the properties of the resulting sensor could be tuned, and additional requirements such as biocompatibility could be achieved. However, the nanofillers are typically randomly orientated and distributed, if no other method is taken. This could limit the performance and functionality (for example, multi-directional sensing) of the fabricated sensor. Furthermore, by adding sacrificial fillers and an etching step, porosity could be introduced within the material system. The added microstructure could help increasing both the flexibility and sensitivity, while more complex methods are required to control the specific size distribution of the microstructures, as discussed below.

To improve the fabrication precision and add designed architectures, micro/nanofabrication is generally needed, which is another technology widely utilized in architected piezoresistive sensors fabrication processes. With great precision, micro/nanofabrication technology, such as photo/electron lithography, could fabricate devices with micro/nanoscale structures, providing the possibility to fabricate integrated piezoresistive sensors with high density. Besides, micro/nanofabrication technology could give significant structural complexity and hierarchy in fabricating functional piezoresistive sensors. Thus, compared with other approaches, micro/nanofabrication technology offers piezoresistive sensors better performance with higher degree of functionality and small sizes. However, micro/nanofabrication technology typically has higher cost and requires more steps. Those limitations constrain the efficiency of the fabrication process.

Moreover, additive manufacturing (AM) methods could give new opportunities in fabricating multi-functional piezoresistive sensors covering a broader range of pressure and stimuli from their capability to generate features made of multi-materials at multiple length scales. For example, by using direct ink writing and/or ink-jet printing method, the active electrical sensing components can be directly printed on substrates to integrate electronics with desired layouts and structures.[227–229] Though the AM technology will not change the material's intrinsic sensitivity, the added porosity or architecture could help improving sensors' performance. Compared to other approaches, AM is highly automated, and the process requires minimal training. Also, AM could provide more versatilities in designing sensor structures, and different AM methods can accommodate various sizes and precision requirements. However, currently there are limited functional materials that are compatible with 3D printing. So, more studies are needed to overcome the current challenges and expand fabrication options and sensing capabilities.

There are also many challenges remaining in the implementation of flexible and stretchable piezoresistive sensors for practical wearable sensing applications, as shown in Fig. 16. The primary drawback of the piezoresistive sensors is that they need a power source. The piezoresistive sensors require an external power source to drive the resistance signal detection process. Therefore, there is a grand challenge in the integration of the piezoresistive sensors with power generation and storage devices. As discussed above, though the piezoelectric and triboelectric materials/structures have many

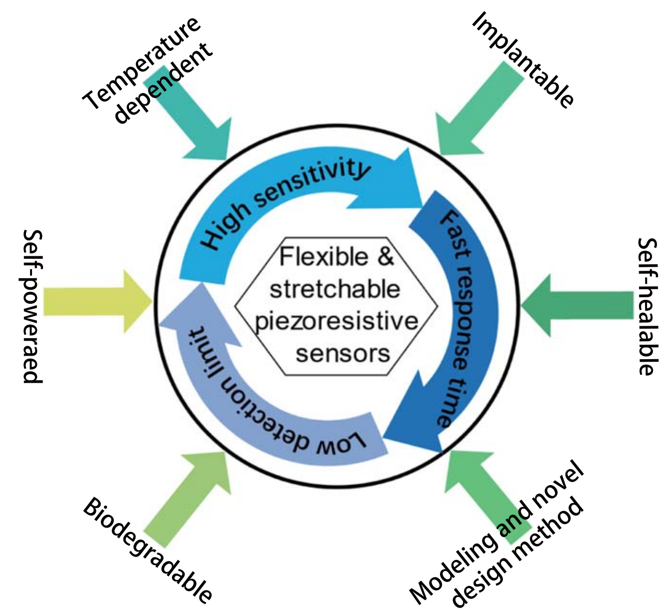

Figure 16. Current challenges and future opportunities for the piezoresistive sensors.

limitations for pressure sensing applications (such as detecting subtle and/or static mechanical loadings), they possess unique charge generation feature which can be used to provide sustainable power for the sensor systems. For achieving this goal, further investigations are needed to incorporate a piezoelectric/triboelectric energy generating unit with a piezoresistive sensing unit for highly sensitive and self-powered sensor systems.

Importantly, most of the recently reported wearable piezoresistive sensors rely on electrically conductive elements coupled with stretchable polymeric materials. However, the mechanical response of these viscoelastic polymeric materials is temperature-dependent, and the conductivity of the electrical elements would be changed with the variation of the ambient temperature as well. This characteristic makes the sensing performance of the piezoresistive sensors temperature dependent, which is a challenge for the practical applications of these sensors under various temperature conditions. Thus, the temperature compensation feature of the piezoresistive sensors should be further investigated, especially for locations where the temperature changes over the sensing cycles.

With the rapid development of electronic technologies, sensor systems are expected to mimic the comprehensive properties of human skin by converting external stimuli into electrical signals. Due to the high sensitivity, ultra-low detection limit and fast response time, the flexible and stretchable piezoresistive sensors are promising candidates for electronic-skin (e-skin) applications. Although the existing piezoresistive sensors are capable of detecting touch, pressure, and strain, multiple sensors are needed to distinguish different physical stimuli (especially for touch and pressure)[230,231] for the comfortable interactions with biological organs.[232,233] Beyond these issues, to detect human physiological information within a body, the implanted piezoresistive sensors need to accurately sense the physical stimuli and wirelessly transmit the electrical signals to receivers. Thus, the piezoresistive sensors should be packaged with the wireless data recorder and transmission units. Therefore, the development of implantable piezoresistive sensors and the corresponding packaging techniques would be needed for e-skin applications.

Moreover, self-healing and biodegradability are the other equally important characteristics of e-skin applications, which can automatically repair when mechanical damages occur and avoid the secondary damage from surgical extraction. As discussed above, the self-healing and biodegradable properties have been achieved using the functionalized elastomer matrices or substrate.[57,111,112,234]

However, the challenge still remains is to realize excellent electromechanical performances and the skin-like features simultaneously.

Furthermore, another grand challenge is establishing multiphysics analytical and numerical models for understanding and predicting the correlation between the material compositions/structures and the electromechanical performances of the piezoresistive sensors. Despite the fact that the sensing mechanisms of each type of piezoresistive sensors are well-known, the existing models have limited success in describing and quantifying the piezoresistive response of these sensors. Machine learning-based approaches such as deep learning, a breakthrough technology for data analysis, can be used to process the detected electrical signals from the piezoresistive sensors via deep neural networks for the exact touch/pressure recognitions.[235] In the future, it might be possible that the highly sophisticated sensing capabilities of the human skin can be imitated by simple materials. However, the deep neural networks of deep learning need extensive training and test data, which are currently very limited. With the rapid progress in the availability of big data, the deep learning-aided sensor systems would be possible in the near future, which can bring new opportunities for the next generation of smart and intelligent wearable sensors.

Acknowledgments

This work was partially supported by the start-up funds from the School of Mechanical Engineering at Hubei University of Technology (BSQD2019010) and the Whiting School of Engineering at Johns Hopkins University, and the Office of Naval Research (Award No.: N00014-19-1-2673).

References

1. Y. Gao, L. Yu, J. C. Yeo, and C. T. Lim, *Adv. Mater.*, **31**, 1902133 (2019).
2. Y. P. Zang, F. J. Zhang, C. A. Di, and D. B. Zhu, *Mater. Horiz.*, **2**, 140 (2015).
3. M. Amjadi, K. U. Kyung, I. Park, and M. Sitti, *Adv. Funct. Mater.*, **26**, 1678 (2016).
4. P. Rai, S. Oh, P. Shyamkumar, M. Ramasamy, R. E. Harbaugh, and V. K. Varadan, *J. Electrochem. Soc.*, **161**, B3116 (2013).
5. T. Q. Trung and N. E. Lee, *Adv. Mater.*, **28**, 201504244 (2016).
6. Y. Ma et al., *Adv. Mater.*, **31**, 1902062 (2019).
7. D. Chung and B. L. Gray, *J. Electrochem. Soc.*, **166**, B3116 (2019).
8. X. Wang, L. Dong, H. Zhang, R. Yu, C. Pan, and Z. L. Wang, *Adv. Sci.*, **2**, 1500169 (2015).
9. C. Pang, G. Y. Lee, T. I. Kim, S. M. Kim, H. N. Kim, S. H. Ahn, and K. Y. Suh, *Nat. Mater.*, **11**, 795 (2012).
10. S. Jung, J. H. Kim, J. Kim, S. Choi, J. Lee, I. Park, T. Hyon, and D. H. Kim, *Adv. Mater.*, **26**, 4825 (2014).
11. D. Kang, P. V. Pikhitsa, Y. W. Choi, C. Lee, and M. Choi, *Nature*, **516**, 222 (2014).
12. B. H. Tok and Z. Bao, *Sci. China Chem.*, **55**, 718 (2012).
13. J. Li, Z. Zhu, L. Fang, S. Guo, U. Erturun, Z. Zhu, J. West, S. Ghosh, and S. H. Kang, *Nanoscale*, **9**, 14215 (2017).
14. J. Chen, H. Liu, W. Wang, N. Nabulsi, W. Zhao, J. Y. Kim, M. K. Kwon, and J. H. Ryou, *Adv. Funct. Mater.*, **29**, 1903162 (2019).
15. U. Khan, T. H. Kim, H. Ryu, W. Seung, and S. W. Kim, *Adv. Mater.*, **29**, 1603544 (2018).
16. X. S. Zhang, M. Han, B. Kim, J. F. Bao, J. Brugger, and H. Zhang, *Nano Energy*, **47**, 410 (2018).
17. G. Schwartz, B. C. K. Tee, J. G. Mei, A. L. Appleton, D. H. Kim, H. L. Wang, and Z. N. Bao, *Nat. Commun.*, **4**, 1859 (2013).
18. S. C. B. Mannsfeld, C. K. Tee, R. M. Stoltenberg, H. H. Chen, S. Barman, B. V. O. Muir, A. N. Sokolov, C. Reese, and Z. Bao, *Nat. Mater.*, **9**, 859 (2010).
19. Y. Ling, X. Zhuang, Z. Xu, Y. Xie, X. Zhu, Y. Xu, B. Sun, J. Lin, Y. Zhang, and Z. Yan, *ACS Nano*, **12**, 12456 (2018).
20. Y. Wei, S. Chen, X. Dong, Y. Lin, and L. Liu, *Carbon*, **113**, 395 (2017).
21. H. Liu, M. Y. Dong, W. J. Huang, J. C. Gao, K. Dai, J. Guo, G. Q. Zheng, C. T. Liu, C. Y. Shen, and Z. H. Guo, *J. Mater. Chem. C*, **5**, 73 (2017).
22. B. Sun, R. N. McCay, S. Goswami, Y. Xu, C. Zhang, Y. Ling, J. Lin, and Z. Yan, *Adv. Mater.*, **30**, 1804327 (2018).
23. R. Takpara, M. Duquennoy, M. Ouaftouh, C. Courtois, Frédéric Jenot, and M. Rguiti, *Ultrasonics*, **79**, 96 (2017).
24. N. R. Alluri, S. Selvarajan, A. Chandrasekhar, B. Saravanakumar, J. H. Jeong, and S. J. Kim, *Compos. Sci. Technol.*, **142**, 65 (2017).
25. W. Deng, L. Jin, B. Zhang, Y. Chen, and Y. Weiqing, *Nanoscale*, **8**, 16302 (2016).
26. Y. Xin, X. Qi, H. Tian, C. Guo, and C. Wang, *Mater. Lett.*, **164**, 136 (2015).
27. J. Zhu, L. Jia, and R. Huang, *J. Mater. Sci., Mater. Electron.*, **28**, 12080 (2017).
28. W. R. Mccall, K. Kim, C. Heath, G. L. Pierre, and D. J. Sirbuly, *ACS Appl. Mater. Interfaces*, **6**, 19504 (2014).
29. N. R. Alluri, V. Vivekananthan, A. Chandrasekhar, and S. J. Kim, *Nanoscale*, **10**, 907 (2018).
30. S. Wang, *IEEE Trans. Biomed. Circuits Syst.*, **10**, 25 (2015).
31. L. Pan, A. Chortos, G. Yu, Y. Wang, S. Isaacson, R. Allen, Y. Shi, R. H. Dauskardt, and Z. N. Bao, *Nat. Commun.*, **5**, 3002 (2014).
32. Y. Yue et al., *Nano Energy*, **50**, 79 (2018).
33. B. Su, S. Gong, Z. Ma, L. W. Yap, and W. Cheng, *Small*, **11**, 1886 (2015).
34. W. Liu, N. Liu, Y. Yue, J. Rao, and Y. Gao, *Small*, **14**, 1704149 (2018).
35. L. H. Yu et al., *Nano Res.*, **12**, 331 (2019).
36. M. Liu, X. Pu, C. Jiang, T. Liu, X. Huang, L. Chen, C. Du, J. Sun, W. Hu, and Z. Lin Wang, *Adv. Mater.*, **29**, 1703700 (2017).
37. S. H. Zhang, L. Zhang, L. Wang, F. Wang, and G. B. Pan, *J. Mater. Chem. C*, **7**, 4760 (2019).
38. S. Kim, Y. Dong, M. M. Hossain, S. Gorman, I. Towfeeq, D. R. Gajula, A. Childress, A. M. Rao, and G. Koley, *ACS Appl. Mater. Interfaces*, **11**, 16006 (2019).
39. W. Deng et al., *Nano Energy*, **55**, 516 (2019).
40. Z. Chen, Z. Wang, X. Li, Y. Lin, N. Luo, M. Long, N. Zhao, and J. B. Xu, *ACS Nano*, **11**, 4507 (2017).
41. R. Li, Y. Si, Z. Zhu, Y. Guo, Y. Zhang, N. Pan, G. Sun, and T. Pan, *Adv. Mater.*, **29**, 1700253 (2017).
42. Z. Zhu, R. Li, and T. Pan, *Adv. Mater.*, **30**, 1705122 (2017).
43. Y. Joo, J. Byun, N. Seong, J. Ha, H. Kim, S. Kim, T. Kim, H. Im, D. Kim, and Y. Hong, *Nanoscale*, **7**, 6208 (2015).
44. T. Li, H. Luo, L. Qin, X. W. Wang, Z. P. Xiong, H. Y. Ding, Y. Gu, Z. Liu, and T. Zhang, *Small*, **12**, 5042 (2016).
45. S. Dai, S. Wang, H. Yan, J. Xu, H. Hu, J. Ding, and N. Yuan, *Mater. Res. Express*, **6**, 0850b9 (2019).
46. Y. Shu et al., *Nanoscale*, **7**, 8636 (2015).
47. J. Shi, L. Wang, Z. Dai, L. Zhao, M. Du, H. Li, and Y. Fang, *Small*, **14**, e1800819 (2018).
48. X. Liu, M. Mwangi, X. Li, M. O'Brien, and G. M. Whitesides, *Lab Chip*, **11**, 2189 (2011).
49. S. Stassi, V. Cauda, G. Canavese, and C. Pirri, *Sensors*, **14**, 5296 (2014).
50. A. V. Tran, X. Zhang, and B. Zhu, *IEEE Trans. Ind. Electron.*, **65**, 6487 (2018).
51. R. Gaska, M. S. Shur, A. D. Bykhovski, J. W. Yang, M. A. Khan, V. V. Kaminski, and S. M. Soloviov, *Appl. Phys. Lett.*, **76**, 3956 (2000).
52. C. Abels, V. Mastronardi, F. Guido, T. Dattoma, A. Qualtieri, W. Megill, M. De Vittorio, and F. Rizzi, *Sensors*, **17**, 1080 (2017).
53. M. Park, J. Park, and U. Jeong, *Nano Today*, **9**, 244 (2014).
54. M. Park, H. Kim, and J. P. Youngblood, *Nanotechnology*, **19**, 055705 (2008).
55. S. Xu et al., *Science*, **344**, 70 (2014).
56. H. Zhu et al., *Adv. Funct. Mater.*, **27**, 1606604 (2017).
57. T. Wang, Y. Zhang, Q. Liu, W. Cheng, X. Wang, L. Pan, B. Xu, and H. Xu, *Adv. Funct. Mater.*, **28**, 1705551 (2018).
58. H. Ren et al., *ACS Nano*, **13**, 5541 (2019).
59. Y. Song, H. Chen, Z. Su, X. Chen, L. Miao, J. Zhang, X. Cheng, and H. Zhang, *Small*, **13**, 1702091 (2017).
60. F. A. Khan, C. M. Ajmal, S. Bae, S. Seo, H. Moon, and S. Baik, *Small*, **14**, 1800549 (2018).
61. S. Zhang, H. Liu, S. Yang, X. Shi, D. Zhang, C. Shan, L. Mi, C. Liu, C. Shen, and Z. Guo, *ACS Appl. Mater. Interfaces*, **11**, 10922 (2019).
62. Y. Cao, T. Li, Y. Gu, H. Luo, and T. Zhang, *Small*, **14**, 1703902 (2018).
63. B. Zhu, Y. Ling, L. W. Yap, M. Yang, F. Lin, S. Gong, Y. Wang, T. An, Y. Zhao, and W. Cheng, *ACS Appl. Mater. Interfaces*, **11**, 29014 (2019).
64. K. Xia, C. Wang, M. Jian, Q. Wang, and Y. Zhang, *Nano Res.*, **11**, 1124 (2018).
65. L. Gao, C. Zhu, L. Li, C. Zhang, J. Liu, H. D. Yu, and W. Huang, *ACS Appl. Mater. Interfaces*, **11**, 25034 (2019).
66. X. W. Wang, Y. Gu, Z. P. Xiong, Z. Cui, and T. Zhang, *Adv. Mater.*, **26**, 1336 (2014).
67. D. Lee, H. Lee, Y. Jeong, Y. Ahn, G. Nam, and Y. Lee, *Adv. Mater.*, **28**, 9364 (2016).
68. W. J. Liu, N. S. Liu, Y. Yue, J. Y. Rao, C. Luo, H. Zhang, C. X. Yang, J. Su, Z. T. Liu, and Y. H. Gao, *J. Mater. Chem. C*, **6**, 1451 (2018).
69. L. Qiu, C. M. Bulut, Y. Tang, J. Z. Liu, T. Alan, J. Ding, V. T. Truong, and D. Jin, *Adv. Mater.*, **28**, 194 (2016).
70. Q. Shao, Z. Niu, M. Hirtz, L. Jiang, Y. Liu, Z. Wang, and X. Chen, *Small*, **10**, 1466 (2014).
71. L. Ma, X. Shuail, P. Zhu, and R. Sun, *18th Int. Conf. on Electronic Packaging Technology*1366 (2017).
72. S. Zhao et al., *ACS Appl. Mater. Interfaces*, **9**, 12147 (2017).
73. Z. Wang and X. Ye, *Nanotechnology*, **24**, 265704 (2013).
74. N. Hu, Y. Karube, M. Arai, T. Watanabe, C. Ya, Y. Li, Y. Liu, and H. Fukunaga, *Carbon*, **48**, 680 (2010).
75. H. B. Yao, J. Ge, C. F. Wang, X. Wang, W. Hu, Z. J. Zheng, Y. Ni, and S. H. Yu, *Adv. Mater.*, **25**, 6692 (2013).
76. J. Park, J. Kim, J. Hong, H. Lee, Y. Lee, S. Cho, S. W. Kim, J. J. Kim, S. Y. Kim, and H. Ko, *NPG Asia Mater.*, **10**, 163 (2018).
77. Y. Lu, M. Tian, X. Sun, N. Pan, F. Chen, S. Zhu, X. Zhang, and S. Chen, *Compos. Part A Appl. Sci. Manuf.*, **117**, 202 (2019).
78. P. Avouris and R. Martel, *MRS Bull.*, **35**, 306 (2010).
79. M. Tabib-Azar, Y. Xie, and R. Wang, *ECS Trans.*, **3**, 437 (2006).
80. D. J. Lipomi, M. Vosgueritchian, B. C. K. Tee, S. L. Hellstrom, J. A. Lee, C. H. Fox, and Z. N. Bao, *Nat. Nanotechnol.*, **6**, 788 (2011).
81. X. Wang, J. F. Li, H. N. Song, H. L. Huang, and J. H. Gou, *ACS Appl. Mater. Interfaces*, **10**, 7371 (2018).

82. M. Amjadi, Y. J. Yoon, and I. Park, *Nanotechnology*, **26**, 375501 (2015).
83. Y. T. Jiang, Y. Wang, Y. K. Mishra, R. R. Adelung, and Y. Yang, *Adv. Mater. Technol.*, **3**, 1800248 (2018).
84. E. Roh, B. Hwang, D. Kim, B. Kim, and N. Lee, *ACS Nano*, **9**, 6252 (2015).
85. H. Liu, J. C. Gao, W. J. Huang, K. Dai, G. Q. Zheng, C. T. Liu, C. Y. Shen, X. R. Yan, J. Guo, and Z. H. Guo, *Nanoscale*, **8**, 12977 (2016).
86. A. Sanli, C. Mueller, O. Kanoun, C. Elibol, and M. F. X. Wagner, *Compos. Sci. Technol.*, **122**, 18 (2016).
87. X. H. Cao, X. D. Wei, G. J. Li, C. Hu, K. Dai, J. Guo, G. Q. Zheng, C. T. Liu, C. Y. Shen, and Z. H. Guo, *Polymer*, **112**, 1 (2017).
88. K. Ke, P. Poetschke, N. Wiegand, B. Krause, and B. Voit, *ACS Appl. Mater. Interfaces*, **8**, 14190 (2016).
89. K. Khanafer, A. Duprey, M. Schlicht, and R. Berguer, *Biomed. Microdevices*, **11**, 503 (2009).
90. C. H. Hu, C. H. Liu, L. Z. Chen, Y. C. Peng, and S. S. Fan, *Appl. Phys. Lett.*, **93**, 1387 (2008).
91. M. Wang, K. Zhang, X. X. Dai, Y. Li, J. Guo, H. Liu, G. H. Li, Y. J. Tan, J. B. Zheng, and Z. Guo, *Nanoscale*, **9**, 11017 (2017).
92. Y. J. Zheng, Y. L. Li, K. Dai, Y. Wang, G. Q. Zheng, C. T. Liu, and C. Y. Shen, *Compos. Sci. Technol.*, **156**, 276 (2018).
93. H. Mai, R. Mutlu, C. Tawk, G. Alici, and V. Sencadas, *Compos. Sci. Technol.*, **173**, 118 (2019).
94. X. H. Liu, W. Liu, Q. Xia, J. H. Feng, Y. P. Qiu, and F. J. Xu, *Compos. Part A Appl. Sci. Manuf.*, **121**, 123 (2019).
95. J. O. Akindoyo, M. D. H. Beg, S. Ghazali, M. R. Islam, N. Jeyaratnam, and A. R. Yuvaraj, *RSC Adv.*, **6**, 114453 (2016).
96. N. Domun, H. Hadavinia, T. Zhang, T. Sainsbury, G. H. Liaghat, and S. Vahid, *Nanoscale*, **7**, 10294 (2015).
97. H. Gu, Y. Zhao, and M. L. Wang, *Struct. Control Hlth.*, **12**, 329 (2005).
98. M. J. Allen, V. C. Tung, and R. B. Kaner, *Chem. Rev.*, **110**, 132 (2010).
99. V. B. Mohan, K. Lau, D. Hui, and D. Bhattacharyya, *Compos. Part B Eng.*, **142**, 200 (2018).
100. D. Niu, W. T. Jiang, G. Y. Ye, K. Wang, L. Yin, Y. S. Shi, B. B. Chen, F. Luo, and H. H. Liu, *Mater. Res. Bull.*, **102**, 92 (2018).
101. M. Östling, A. D. Smith, S. Vaziri, S. S. Delekta, J. Li, and M. C. Lemme, *ECS Trans.*, **75**, 17 (2016).
102. G. Rajitha and R. K. Dash, *Sens. Actuators A*, **277**, 26 (2018).
103. T. T. Yang, X. Jiang, Y. Y. Zhong, X. L. Zhao, S. Y. Lin, J. Li, X. X. Li, J. L. Xu, Z. H. Li, and H. W. Zhu, *ACS Sensors*, **2**, 967 (2017).
104. J. H. Li, S. F. Zhao, X. L. Zeng, W. P. Huang, Z. Y. Gong, G. P. Zhang, R. Sun, and C. P. Wong, *ACS Appl. Mater. Interfaces*, **8**, 18954 (2016).
105. C. S. Boland et al., *Science*, **354**, 1257 (2016).
106. P. Costa, J. Nunes-Pereira, J. Oliveira, J. Silva, J. Agostinho Moreira, S. A. C. Carabineiro, J. G. Buijnsters, and S. Lanceros-Mendez, *Compos. Sci. Technol.*, **153**, 241 (2017).
107. V. Eswaraiah, K. Balasubramaniam, and S. Ramaprabhu, *Nanoscale*, **4**, 1258 (2012).
108. F. Wang, S. Zhang, L. Wang, Y. Zhang, J. Lin, X. Zhang, T. Chen, Y. Lai, G. Pan, and L. Sun, *J. Mater. Chem. C*, **6**, 12575 (2018).
109. D. Zhang, K. W. Zhang, Y. M. Wang, Y. H. Wang, and Y. Yang, *Nano Energy*, **56**, 25 (2019).
110. Y. M. Wang, Y. Wang, and Y. Yang, *Adv. Energy Mater.*, **8**, 1800961 (2018).
111. R. Scaffaro, A. Maio, G. Lo Re, A. Parisi, and A. Busacca, *Compos. Sci. Technol.*, **156**, 166 (2018).
112. L. W. Zhao, B. Jiang, and Y. D. Huang, *J. Mater. Sci.*, **54**, 5472 (2019).
113. S. Chen, K. Jiang, Z. Lou, D. Chen, and G. Shen, *Adv. Mater. Technol.*, **3**, 1700248 (2017).
114. Z. Yang et al., *ACS Appl. Mater. Interfaces*, **10**, 3948 (2018).
115. Z. H. Wu, C. Xu, C. Q. Ma, Z. B. Liu, H. M. Cheng, and W. C. Ren, *Adv. Mater.*, **31**, 1900199 (2019).
116. N. Q. Luo, Y. Huang, J. Liu, S. C. Chen, C. P. Wong, and N. Zhao, *Adv. Mater.*, **29**, 1702675 (2017).
117. K. Huang, S. M. Dong, J. S. Yang, J. Y. Yan, Y. D. Xue, X. You, J. B. Hu, L. Gao, X. Y. Zhang, and Y. S. Ding, *Carbon*, **143**, 63 (2019).
118. Y. G. Hu, T. Zhao, P. L. Zhu, Y. Zhang, X. W. Liang, R. Sun, and C. P. Wong, *Nano Research*, **11**, 1938 (2018).
119. S. Lee, J. Koo, S. Kang, G. G. Park, Y. J. Lee, Y. Y. Chen, S. A. Lim, K. M. Lee, and J. A. Rogers, *Mater. Today*, **21**, 207 (2018).
120. K. H. Kim, N. S. Jang, S. H. Ha, J. H. Cho, and J. M. Kim, *Small*, **14**, 1704232 (2018).
121. T. Hu, S. H. Xuan, L. Ding, and X. L. Gong, *Mater. Des.*, **156**, 528 (2018).
122. X. J. Xu, R. R. Wang, P. Nie, Y. Cheng, X. Y. Lu, L. J. Shi, and J. Sun, *ACS Appl. Mater. Interfaces*, **9**, 14273 (2017).
123. M. D. Ho, Y. Z. Ling, L. W. Yap, Y. Wang, D. Dong, Y. M. Zhao, and W. L. Cheng, *Adv. Funct. Mater.*, **27**, 1700845 (2017).
124. M. Z. Seyedin, J. M. Razal, P. C. Innis, and G. G. Wallace, *Adv. Funct. Mater.*, **24**, 2957 (2014).
125. Y. Wang et al., *Sci. Adv.*, **3**, e1602076 (2017).
126. L. L. Wang, J. A. Jackman, E. Tan, J. H. Park, M. G. Potroz, E. T. Hwang, and N. J. Cho, *Nano Energy*, **36**, 38 (2017).
127. B. Gray, *ECS Trans.*, **28**, 535 (2010).
128. J. Wang, W. Ding, S. Lv, J. Wan, and Z. Hu, *J. Electrochem. Soc.*, **165**, B924 (2018).
129. Y. Kervran, K. Kandoussi, H. Dong, S. Janfaoui, N. Coulon, C. Simon, E. Jacques, and T. Mohammed-Brahim, *ECS Trans.*, **75**, 13 (2016).
130. F. Garcia-Castro, O. De Sagazan, C. Simon, N. Coulon, and F. Le Bihan, *ECS Trans.*, **86**, 71 (2018).
131. Z. Wang, R. Jiang, G. Li, Y. Chen, Z. Tang, Y. Wang, Z. Liu, H. Jiang, and C. Zhi, *ACS Appl. Mater. Interfaces*, **9**, 22685 (2017).
132. V. Chabot, D. Higgins, A. P. Yu, X. C. Xiao, Z. W. Chen, and J. J. Zhang, *Energy Environ. Sci.*, **7**, 1564 (2014).
133. Y. C. Ding, T. Xu, O. Onyilagha, H. Fong, and Z. T. Zhu, *ACS Appl. Mater. Interfaces*, **11**, 6685 (2019).
134. S. S. Xiao, H. Mei, D. Y. Han, K. G. Dassios, and L. F. Cheng, *Carbon*, **122**, 718 (2017).
135. H. Wang, W. B. Lu, J. T. Di, D. Li, X. H. Zhang, M. Li, Z. G. Zhang, L. X. Zheng, and Q. W. Li, *Adv. Funct. Mater.*, **27**, 1606220 (2017).
136. M. Jahanbakhshi, *Mater. Sci. Eng. C Mater. Bio. Appl.*, **70**, 544 (2017).
137. J. Kuang, L. Q. Liu, Y. Gao, D. Zhou, Z. Chen, B. H. Han, and Z. Zhang, *Nanoscale*, **5**, 12171 (2013).
138. B. W. Yao, J. Chen, L. Huang, Q. Q. Zhou, and G. Q. Shi, *Adv. Mater.*, **28**, 1623 (2016).
139. Y. X. Ma, M. Yu, J. H. Liu, X. J. Li, and S. M. Li, *ACS Appl. Mater. Interfaces*, **9**, 27127 (2017).
140. J. H. Li, S. F. Zhao, G. P. Zhang, Y. J. Gao, L. B. Deng, R. Sun, and C. P. Wong, *J. Mater. Chem. A*, **3**, 15482 (2015).
141. C. J. Chen et al., *Chem*, **4**, 544 (2018).
142. M. Inagaki, J. S. Qiu, and Q. G. Guo, *Carbon*, **87**, 128 (2015).
143. Y. A. Samad, Y. Q. Li, S. M. Alhassan, and K. Liao, *ACS Appl. Mater. Interfaces*, **7**, 9195 (2015).
144. Y. A. Samad, Y. Q. Li, A. Schiffer, S. M. Alhassan, and K. Liao, *Small*, **11**, 2380 (2015).
145. M. X. Xu, F. Li, Z. Y. Zhang, T. Shen, and J. J. Qi, *Adv. Electron. Mater.*, **5**, 1800461 (2019).
146. J. X. Huang, H. G. Wang, Z. P. Li, X. Z. Wu, J. Q. Wang, and S. R. Yang, *J. Mater. Chem. C*, **7**, 7386 (2019).
147. X. G. Yu, Y. Q. Li, W. B. Zhu, P. Huang, T. T. Wang, N. Hu, and S. Y. Fu, *Nanoscale*, **9**, 6680 (2017).
148. J. W. Song et al., *Nature*, **554**, 224 (2018).
149. Z. Lin, Z. Zeng, X. Gui, Z. Tang, and A. Cao, *Adv. Energy Mater.*, **6**, 1600554 (2016).
150. G. Tong, F. Du, L. Xiang, F. Liu, and J. Guan, *Nanoscale*, **6**, 778 (2013).
151. S. Y. Wu, J. Zhang, R. B. Ladani, A. R. Ravindran, A. P. Mouritz, A. J. Kinloch, and C. H. Wang, *ACS Appl. Mater. Interfaces*, **9**, 14207 (2017).
152. S. Garlof, T. Fukuda, M. Mecklenburg, D. Smazna, Y. K. Mishra, R. Adelung, K. Schulte, and B. Fiedler, *Compos. Sci. Technol.*, **134**, 226 (2016).
153. Y. Li, D. Han, C. Jiang, E. Xie, and W. Han, *Adv. Mater. Technol.*, **4**, 1800504 (2019).
154. L. Yang, R. Wang, Q. Song, Y. Liu, Q. Zhao, and Y. Shen, *Compos. Part A Appl. Sci. Manuf.*, **101**, 195 (2017).
155. J. Li, S. Orrego, J. Pan, P. He, and S. H. Kang, *Nanoscale*, **11**, 2779 (2019).
156. W. J. Huang, K. Dai, Y. Zhai, H. Liu, P. F. Zhan, J. C. Gao, G. Q. Zheng, C. T. Liu, and C. Y. Shen, *ACS Appl. Mater. Interfaces*, **9**, 42266 (2017).
157. S. Wu, R. B. Ladani, J. Zhang, K. Ghorbani, X. Zhang, A. P. Mouritz, A. J. Kinloch, and C. H. Wang, *ACS Appl. Mater. Interfaces*, **8**, 24853 (2016).
158. W. N. He, G. Y. Li, S. Q. Zhang, Y. Wei, J. Wang, Q. W. Li, and X. T. Zhang, *ACS Nano*, **9**, 4244 (2015).
159. F. Wang, Y. Wang, W. Zhan, S. Yu, W. Zhong, G. Sui, and X. Yang, *Chem. Eng. J.*, **320**, 539 (2017).
160. M. Luo, M. Li, Y. Li, K. Chang, K. Liu, Q. Liu, Y. Wang, Z. Lu, X. Liu, and D. Wang, *Compos. Commun.*, **6**, 68 (2017).
161. G. Ge, Y. Cai, Q. Dong, Y. Zhang, J. Shao, W. Huang, and X. Dong, *Nanoscale*, **10**, 10033 (2018).
162. Y. H. Wu, H. Z. Liu, S. Chen, X. Dong, P. P. Wang, S. Liu, Y. Liu, Y. Wei, and L. Liu, *ACS Appl. Mater. Interfaces*, **9**, 20098 (2017).
163. M. Langner, S. Agarwal, A. Baudler, U. Schroder, and A. Greiner, *Adv. Funct. Mater.*, **25**, 6182 (2015).
164. M. E. D. Asaro, M. S. Otten, S. Chen, and J. H. Lang, *J. Appl. Polym. Sci.*, **134** (2017).
165. X. Wu, Y. Han, X. Zhang, Z. Zhou, and C. Lu, *Adv. Funct. Mater.*, **26**, 1601995 (2016).
166. A. Tewari, S. Gandla, S. Bohm, C. R. Mcneill, and D. Gupta, *ACS Appl. Mater. Interfaces*, **10**, 5185-5195 (2018).
167. Y. Yue et al., *Nano Energy*, **50**, 79 (2018).
168. Y. Ding, J. Yang, C. Tolle, and Z. Zhu, *ACS Appl. Mater. Interfaces*, **10**, 16077 (2018).
169. H. Zhang et al., *ACS Appl. Mater. Interfaces*, **8**, 22374 (2016).
170. S. Jiang, S. Reich, B. Uch, P. Hu, and A. Greiner, *ACS Appl. Mater. Interfaces*, **9**, 34286 (2017).
171. Z. Ma, A. W, J. Ma, L. Shao, H. Jiang, D. Dong, Z. Ji, Q. Wang, and S. Kanga, *Nanoscale*, **10**, 7116 (2018).
172. Y. Guo, Z. Guo, M. Zhong, P. Wan, W. Zhang, and L. Zhang, *Small*, **14**, 1803018 (2018).
173. S. Liang, Y. Li, J. Yang, J. Zhang, C. He, Y. Liu, and X. Zhou, *Adv. Mater. Technol.*, **1**, 1600117 (2016).
174. A. Lekawa-Raus, K. K. K. Koziol, and A. H. Windle, *ACS Nano*, **8**, 11214 (2014).
175. J. C. Fernandez-Toribio, A. Iniguez-Rabago, J. Vila, C. Gonzalez, A. Ridruejo, and J. J. Vilatela, *Adv. Funct. Mater.*, **26**, 7139 (2016).
176. Y. Li, Y. Shang, X. He, Q. Peng, S. Du, E. Shi, S. Wu, Z. Li, P. Li, and A. Cao, *ACS Nano*, **7**, 8128 (2013).

177. T. Xu, Y. Ding, Z. Wang, Y. Zhao, W. Wu, H. Fong, and Z. Zhu, *J. Mater. Chem. C*, **5**, 10288 (2017).
178. S. Ryu, P. Lee, J. B. Chou, R. Xu, R. Zhao, A. J. Hart, and S.-G. Kim, *ACS Nano*, **9**, 5929 (2015).
179. Y. Cheng, R. Wang, J. Sun, and L. Gao, *Adv. Mater.*, **27**, 7365 (2015).
180. Y. Si, X. Wang, C. Yan, L. Yang, J. Yu, and B. Ding, *Adv. Mater.*, **28**, 9512 (2016).
181. O. Y. Kweon, S. J. Lee, and J. H. Oh, *NPG Asia Mater.*, **10**, 540 (2018).
182. X. Wang, S. Meng, M. Tebyetekerwa, Y. Li, J. Pionteck, B. Sun, Z. Qin, and M. Zhu, *Compos. Part A Appl. Sci. Manuf.*, **105**, 91 (2018).
183. Z. Zhao, B. Li, L. Xu, Y. Qiao, F. Wang, Q. Xia, and Z. Lu, *Polymers*, **10**, 575 (2018).
184. Y. Liu, K. He, G. Chen, W. R. Leow, and X. Chen, *Chem. Rev.*, **117**, 12893 (2017).
185. C. Wang, C. Wang, Z. Huang, and S. Xu, *Adv. Mater.*, **30**, 1801368 (2018).
186. Y. Huang, X. Fan, S. C. Chen, and N. Zhao, *Adv. Funct. Mater.*, **29**, 1808509 (2019).
187. J. Ashmore, *Physiol. Rev.*, **88**, 173 (2008).
188. C. Pang, T. Kim, W. G. Bae, D. Kang, S. M. Kim, and K. Y. Suh, *Adv. Mater.*, **24**, 475 (2012).
189. J. Park, Y. Lee, J. Hong, Y. Lee, M. Ha, Y. Jung, H. Lim, S. Y. Kim, and H. Ko, *ACS Nano*, **8**, 12020 (2014).
190. H. H. Chou, A. Nguyen, A. Chortos, J. W. To, C. Lu, J. Mei, T. Kurosawa, W. G. Bae, J. B. Tok, and Z. Bao, *Nat. Commun.*, **6**, 8011 (2015).
191. X. Wang, Y. Gu, Z. Xiong, Z. Cui, and T. Zhang, *Adv. Mater.*, **26**, 1336 (2014).
192. N. Cauna, *Anatomical Rec.*, **119**, 449 (1954).
193. J. Park, Y. Lee, J. Hong, M. Ha, Y. D. Jung, H. Lim, S. Y. Kim, and H. Ko, *ACS Nano*, **8**, 4689 (2014).
194. J. Park, M. Kim, Y. Lee, H. S. Lee, and H. Ko, *Sci. Adv.*, **1**, 1500661 (2015).
195. K. Wang, Z. Lou, L. Wang, L. Zhao, S. Zhao, D. Wang, W. Han, K. Jiang, and G. Shen, *ACS Nano*, **13**, 9139 (2019).
196. Y. Wei, S. Chen, Y. Lin, Z. Yang, and L. Liu, *J. Mater. Chem. C* , **3**, 9594 (2015).
197. C. K. Tee, A. Chortos, R. R. Dunn, G. Schwartz, E. Eason, and Z. Bao, *Adv. Funct. Mater.*, **24**, 5427 (2014).
198. B. Zhu, Z. Niu, H. Wang, W. R. Leow, H. Wang, Y. Li, L. Zheng, J. Wei, F. Huo, and X. Chen, *Small*, **10**, 3625 (2014).
199. C. L. Choong et al., *Adv. Mater.*, **26**, 3451 (2014).
200. Z. Huang, M. Gao, Z. Yan, T. Pan, S. A. Khan, Y. Zhang, H. Zhang, and Y. Lin, *Sensors Actuators A, Phys.*, **266**, 345 (2017).
201. G. Y. Lee, H. T. Lee, W. Ryu, S. H. Ahn, and J. Yang, *Smart Mater. Struct.*, **27** (2018).
202. W. Zhong, Q. Liu, Y. Wu, Y. Wang, X. Qing, M. Li, K. Li, W. Wang, and D. Wang, *Nanoscale*, **8**, 12105 (2016).
203. S. Park et al., *Adv. Mater.*, **26**, 7324 (2014).
204. N. Khalili, X. Shen, and H. E. Naguib, *Soft Matter*, **14**, 6912 (2018).
205. H. Tian, Y. Shu, X. F. Wang, M. A. Mohammad, Z. Bie, Q. Y. Xie, C. Li, W. T. Mi, Y. Yang, and T. L. Ren, *Sci. Rep.*, **5**, 8603 (2015).
206. Z. Wang et al., *Adv. Mater.*, **30**, 1805630 (2018).
207. H. Li, K. Wu, Z. Xu, Z. Wang, Y. Meng, and L. Li, *ACS Appl. Mater. Interfaces*, **10**, 20826 (2018).
208. S. Peng, P. Blanloeuil, S. Wu, and C. H. Wang, *Adv. Mater. Interfaces*, **5**, 1800403 (2018).
209. M. Ha, S. Lim, J. Park, D. S. Um, Y. Lee, and H. Ko, *Adv. Funct. Mater.*, **25**, 2841 (2015).
210. J. C. Yang, J. O. Kim, J. Oh, S. Y. Kwon, J. Y. Sim, D. W. Kim, H. B. Choi, and S. Park, *ACS Appl. Mater. Interfaces*, **11**, 19472 (2019).
211. F. Xu, X. Wang, Y. Zhu, and Y. Zhu, *Adv. Funct. Mater.*, **22**, 1279 (2012).
212. N. Gao, X. Zhang, S. Liao, H. Jia, and Y. Wang, *ACS Macro Lett.*, **5**, 823 (2016).
213. J. Mu, C. Hou, G. Wang, Q. Zhang, Y. Li, H. Wang, and M. Zhu, *Adv. Mater.*, **28**, 9491 (2016).
214. X. Wei, X. Gao, Y. Wang, G. Zheng, K. Dai, C. Liu, and C. Shen, *Compos. Sci. Technol.*, **149**, 166 (2017).
215. Z. Wang, X. Guan, H. Huang, H. Wang, W. Lin, and Z. Pen, *Adv. Funct. Mater.*, **29**, 1807569 (2019).
216. Y. Wei, S. Chen, X. Yuan, P. Wang, and L. Liu, *Adv. Funct. Mater.*, **26**, 5078 (2016).
217. G. Y. Bae, S. W. Park, D. Kim, G. Lee, D. H. Kim, Y. Chung, and K. Cho, *Adv. Mater.*, **28**, 5300 (2016).
218. G. Yu, J. Hu, Y. Gao, Y. Lu, and F. Xuan, *Nanotechnology*, **29**, 115502 (2018).
219. C. Yang, J. Zhao, J. Wang, J. Xie, Y. Gao, M. Xue, and C. Lu, *ACS Appl. Mater. Interfaces*, **10**, 25811 (2018).
220. L. M. Castano and B. Alison, *Smart Mater. Struct.*, **23**, 053001 (2014).
221. S. V. Lomov, G. Huysmans, Y. Luo, R. S. Parnas, and F. R. Phelan, *Compos. Part A*, **32**, 1379 (2001).
222. M. Liu, X. Pu, C. Jiang, T. Liu, X. Huang, L. Chen, C. Du, J. Sun, W. Hu, and Z. L. Wang, *Adv. Mater.*, **29**, 1703700 (2017).
223. J. Deignan, M. Jacobs, L. Florea, S. Coyle, and R. Paradiso, *2016 IEEE SENSORS* (2016).
224. Z. Yang, Y. Pang, X. Han, Y. Yang, J. Ling, M. Jian, Y. Zhang, Y. Yang, and T. Ren, *ACS Nano*, **12**, 9134 (2018).
225. H. Zhang, Z. Shi, M. Zhou, F. Wang, Q. Xia, Y. Qiao, L. Yu, and Z. Lu, *Smart Mater. Struct.*, **27**, 105027 (2018).
226. J. Lee, H. Kwon, J. Seo, J. H. Koo, C. Pang, S. Son, J. H. Kim, Y. H. Jang, D. E. Kim, and T. Lee, *Adv. Mater.*, **27**, 2433 (2015).
227. A. D. Valentine, T. A. Busbee, J. W. Boley, J. R. Raney, A. Chortos, A. Kotikian, J. D. Berrigan, M. F. Durstock, and J. A. Lewis, *Adv. Mater.*, **29**, 1703817 (2017).
228. A. T. Alreshaid, J. G. Hester, W. Su, Y. Fang, and M. M. Tentzeris, *J. Electrochem. Soc.*, **165**, B407 (2018).
229. H. Shamkhalichenar and J.-W. Choi, *J. Electrochem. Soc.*, **164**, B3101 (2017).
230. D. Son et al., *Nat. Nanotechnol.*, **9**, 397 (2014).
231. Y. Yamamoto, S. Harada, D. Yamamoto, W. Honda, T. Arie, S. Akita, and K. Takei, *Sci. Adv.*, **2**, e1601473 (2016).
232. M. Han1 et al., *Nat. Electron.*, **2**, 26 (2019).
233. S. Salminger et al., *Sci. Robot.*, **4**, eaaw6306 (2019).
234. S. Salminger et al., *Nature*, **530**, 71 (2016).
235. K. S. Sohn, J. Chung, M. Y. Cho, S. Timilsina, W. B. Park, M. Pyo, N. Shin, K. Sohn, and J. S. Kim, *Sci. Rep.*, **7**, 11061 (2017).